Heliyon 5 (2019) e02629

Contents lists available at ScienceDirect

Heliyon

journal homepage: www.heliyon.com

Heliyon

Research article

Electrical discharge machining of ceramic nanocomposites: sublimation phenomena and adaptive control

Sergey N. Grigoriev, Mikhail P. Kozochkin, Artur N. Porvatov, Marina A. Volosova, Anna A. Okunkova *

Department of High-Efficiency Machining Technologies, Moscow State University of Technology STANKIN, Vadkovskiy per. 3A, 127055, Moscow, Russian Federation

ARTICLE INFO

Keywords:
Mechanical engineering
Metallurgical engineering
Nanotechnology
Materials science
Conductive ceramics
Wire tool
Discharge gap
Al_2O_3+SiC_w+TiC
Al_2O_3+TiC
Sublimation
Vibrations
Acoustic emission
Monitoring

ABSTRACT

The productivity of electrical discharge machining (EDM) is relatively low owing to the natural laws of electrical erosion. Precise EDM demands uninterrupted control of the discharge gap and adjustment of process parameters. It is particularly critical for processing large workpieces with complex linear surfaces and for materials with threshold conductivities such as the new advanced ceramic nanocomposites Al_2O_3+TiC and Al_2O_3+SiC_w+TiC(30–40%). In these cases, adequate flushing of erosion products is hampered by the geometry of the working space or by the small value of the required discharge gap, which does not exceed 2.2–2.5 μm. The methods of adaptive control in modern computer numerical control systems of EDM equipment based on measuring the electrical parameters in the working zone have been shown to be ineffective in the cases described above. This study aims to investigate the natural phenomena of material sublimation under discharge pulses for conductive ceramics and nanocomposites. The measured conductivities of the samples are higher than the percolation threshold. However, the question of machinability remains open owing to detected processing interruptions and poor quality of machined surfaces. New knowledge on EDM of conductive ceramics and nanocomposites can improve the final quality of the machined surfaces and productivity of the method by the introduction of advanced monitoring and control methods based on acoustic emissions. The manuscript presents an up-to-date overview and current state of the research on the subject area. The obtained morphology of the samples and discussion of the findings complete the experimental part of the study. The scientific basis for a new type of adaptive control system is provided. This can improve the effectiveness of parameter control for machining conductive ceramics and nanocomposites and contribute to an increase in the EDM performance for the most critical cases.

1. Introduction

Electrical discharge machining (EDM) is one of the priciest machining processes for producing metallic parts with complex linear surfaces and roughness *Ra* of up to 0.17–0.2 [1, 2, 3, 4, 5]. Modern computer numerical control (CNC) machines allow producing parts with a positioning accuracy of guiding bars of up to 80 nm [6, 7, 8, 9]. The technology application has been extended significantly by the addition of up to six rotating axes [10, 11]. At the same time, the use of new oil-based ecological dielectrics makes the process even more precise and safer for the environment [12, 13, 14, 15, 16]. However, EDM has low productivity and is applicable only for conductive materials [17, 18, 19, 20].

The low productivity of EDM is related to the natural laws of erosion under discharge current and the auxiliary time related to the work preparation process such as

- time on CNC programming either manually or according to a three-dimensional (3D) model in a computer-aided manufacturing system;
- time on workpiece fastening and locating of the relative coordinate system;
- time on controlling tank flooding and refastening of the workpiece during processing, if necessary, according to the developed technological route; and
- time on resolving manufacturing issues related to wire tool breakage, recharging, impossibility to restart the program at the place of its rupture, returning to the home point, restarting of CNC program, etc.

It is particularly critical in the case of machining an array of narrow

* Corresponding author.
E-mail address: a.okunkova@stankin.ru (A.A. Okunkova).

https://doi.org/10.1016/j.heliyon.2019.e02629
Received 23 October 2018; Received in revised form 26 June 2019; Accepted 7 October 2019

slots for ejector pins of an injector mould [21, 22]. For example, up to 24 tiny slots are required in the form of 1.5 × 8 mm rounded rectangles at the workpiece of 15–25 mm thickness at 100–150 mm of remoteness from a nozzle for producing an injection mould of a car backlight body (Fig. 1). The wire can be blocked during EDM by falling out internal pieces, which can be stuck as well in the lower nozzle of the machine. Blocking of wire tool often leads to undesirable issues related to processing instability, short circuits, and wire breakage. Finally, it influences dramatically the quality of the machined surfaces, which cannot be finished by another machining method due to its small size and inaccessibility [23, 24, 25].

Another case is separating two geometrically mating profiles of an injection mould from a large workpiece with a weight of up to 300 kg used for manufacturing an injection mould of milk bins for transporting dairy products (Fig. 2). It is necessary to control the moment of the final separation of the two workpieces, which are held by a few bridges, to prevent uncontrolled falling into the tank of the machine [26, 27]. The practice of working at EDM machines allows detecting the moment of separation by a specific noise to pause the machine on time for refastening the parts [28, 29]. Similar problems exist in the case of machining a complex linear surface with a variable inclination [30]. During processing, the surface under variable angle flushing of the working zone is not often sufficient and the retained debris hampers the processing, reduces the processing speed, and leads to short circuits. Another big challenge for EDM can be cutting a workpiece with an uneven structure such as a set of hollow tubes or foam-like material or material with varying mesostructure even from the known conductive and easy-to-machine (by EDM) material [31, 32].

The excellent properties of ceramics such as high hardness, resistance to abrasion, erosion, and corrosion, absence of chemical interaction in the working medium and with the environment, and low thermal expansion make them unreplaceable for the aviation and aerospace industry and in other important applications [33, 34, 35, 36, 37, 38, 39, 40]. In medicine, ceramic implants show their reliability, high wear resistance, absence of metal ion accumulation, reduced risk of revision surgery, and negative consequences [41, 42, 43]. However, conventional machining technologies are very costly in the processing of ceramics. Studies [44, 45, 46] have shown and proved the possibility of improving the conductivity of ceramics by conductive additives with no losses on their physical and mechanical properties. The first advanced ceramics based on the commonly known and applicable Al_2O_3+30–40% system of TiC for the production of cutting tools have been available industrially since the early 80s (1981–1984) [47, 48, 49]. Over time, the production methods have been significantly improved by adding more fine-grained phases in the composite based on Al_2O_3 with 30% of TiC and using more advanced methods of pressing and sintering [50, 51]. Researchers have studied the percolation threshold and conductive properties of new advanced ceramics with respect to the proportion of conductive additives [52, 53]. The first studies on samples of composites and nanocomposites of Al_2O_3+TiC system produced by spark plasma sintering (SPS) were reported by the group headed by Prof. Zhang [54, 55, 56]. Then, a research group under the supervision of Prof. Torrecillas and Prof. Moya proposed an advanced SPS method assisted by electrical current to produce new nanocomposites of Al_2O_3+SiC_w+TiC. In addition, the question of the percolation threshold and the achieved electrical and mechanical properties of samples were discussed [57, 58, 59]. Note that having a suitable conductivity for EDM and attaining precise machining are two different things. Since 1997, there have been a few publications related to EDM of a sample made of Al_2O_3+TiC composite [60, 61, 62]. The authors gave recommendations for EDM pulse generator parameters, but a satisfactory quality of machined surface that can be suitable for industrial use was not achieved. The issues on the machinability of Al_2O_3+SiC_w+TiC ceramics by electrical discharge were studied as well by another known scientific group under the supervision of Prof. Pulak M. Pandey [63, 64, 65]. They showed optimised EDM parameters and analysed the surface after EDM. However, the research on EDM of ceramics with a suitable percolation threshold remains at the stage of general electrical parameter definition. Because the issue was already pre-studied experimentally [10, 66, 67, 68], that can be enough for the rough separation of parts. High-precision EDM of conductive ceramic composites and nanocomposites remains a challenging and science-intensive problem.

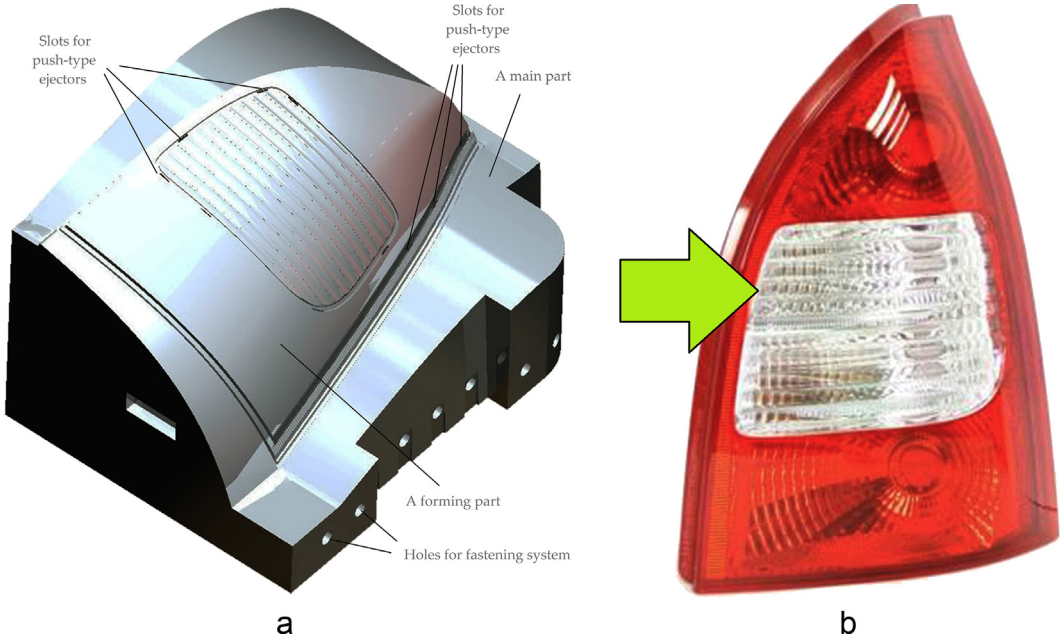

Fig. 1. The body of motor vehicle backlight: (a) A view of the injection mold die with the slots for push-type ejectors designed by JSC IMID (Moscow, Russian Federation); (b) A produced and assembled backlight (Lada Kalina Universal, AvtoVAZ, Tolyatti, Samara region, Russian Federation).

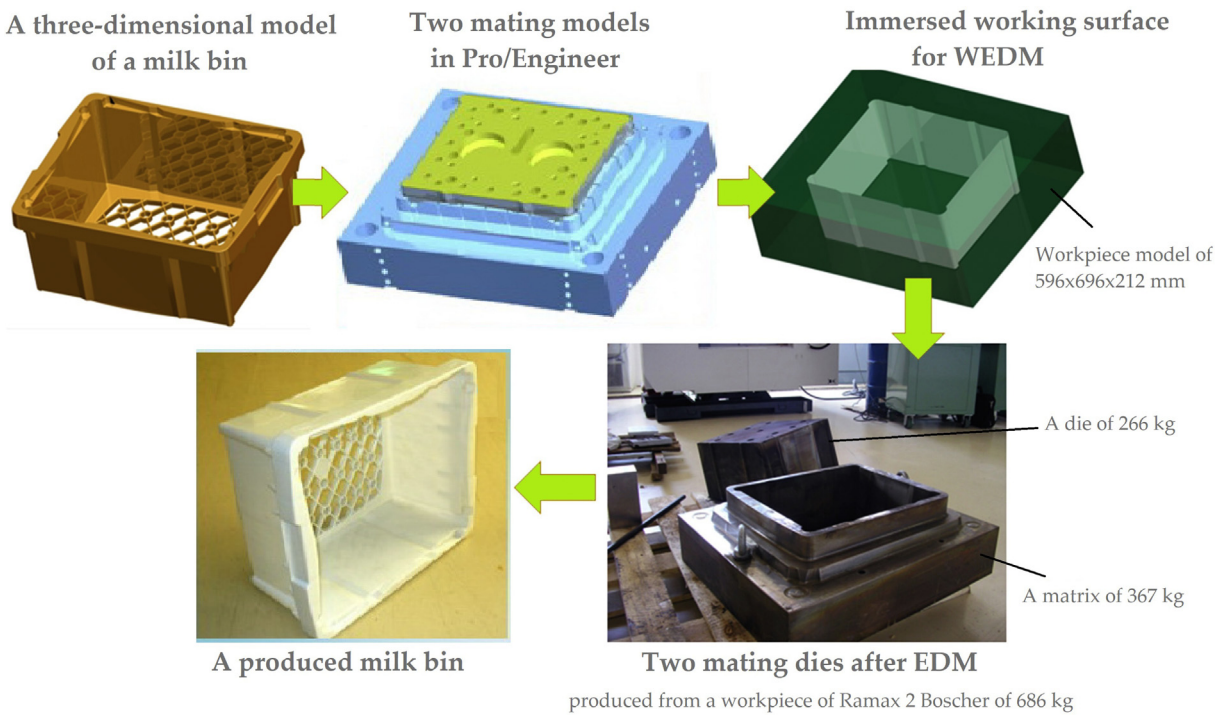

Fig. 2. Schematic diagram of the milk bin production by EDM (JSC IMID, Moscow, Russian Federation).

As it can be seen from the available references, Al_2O_3(+SiC)+TiC composites and nanocomposites obtained by production methods with 30–40% of additives are electrically suitable for EDM. The conductivity of these composites is often higher than the percolation threshold of materials that can be called conductors. Ceramic composites with 40% of conductive additives can have an electrical conductivity close to or even higher than that of hard alloys. Consequently, they should be suitable for EDM as shown in the many studies mentioned above. Nevertheless, in reality, a satisfactory quality of machined surface cannot be achieved.

The above problem can be related mostly to the high thermal resistance of ceramics and the small value of the required discharge gap, which is 15–20 times less than that of conductive materials [69]. The high thermal resistance of ceramics made them unsuitable for conventional approaches in EDM. They need another electrode tool material that is more thermally resistant for a proper combination with the workpiece. In this case, the conventional monitoring and adaptive control systems of EDM based on electrical parameters are unsuitable for the machining of ceramics [70, 71, 72, 73, 74, 75]. Studies [45, 46, 66, 71] that investigated composites with reinforced ferrous matrix and conductive composites based on nitride ceramics demonstrated the typical defects and difficulties in using conventional machining techniques.

As can be observed, being conductive is not sufficient for precision EDM. This research is aimed at revealing the nature of the erosion process of conductive ceramics under discharge current and developing adequate monitoring tools. It is planned to determine a suitable material for the wire tool and estimate the discharge gap.

Note that the EDM process takes place in conditions of full dielectric submersion. The working area is tiny because the discharge gap is approximately 0.045 mm for stainless steel and located at a distance of 1–2 mm from the dielectric level. Additional monitoring methods based on visual access to the working zone are not sufficient, but conventional monitoring methods based on electrical parameters proved to be ineffective [76, 77, 78].

In-situ monitoring based on acoustic emission is shown to be reliable for the requirements of mechanical processing [79, 80, 81, 82]. It can detect the wear rate of cutting tools or unstable conditions of a machine tool during processing. The significant advantage is the simplicity of installation and the possibility of collecting acoustic data remotely. The ability to use acoustic emission for an adaptive control system with higher reliability has been proved [74].

The scientific novelty of this study is the investigation of the natural phenomena of electrical erosion of the electrode materials under discharge current during the processing of conductive ceramic composites and nanocomposites (materials with suitable or threshold conductivities, but high thermal resistances) based on acoustic emission monitoring data and microscopy. The practical importance of the study is the analytical determination of the suitable electrode tool material and appropriate value of the discharge gap, as well as the recommendation on the developed in-situ monitoring method.

The main objectives of the study are as follows:

1) development of an in-situ monitoring method based on acoustic emission for the EDM requirements of samples with complex linear surfaces, uneven mesostructures, and threshold conductivities;
2) applicability of the developed system on samples of industrially obtained ceramic composite Al_2O_3+TiC and advanced ceramic nanocomposite Al_2O_3+SiC_w+TiC;
3) analysis on the nature of oscillations during EDM and productivity of pulses, and investigation of the origin of instability during EDM of conductive ceramics; and
4) determination of a suitable material for the wire tool and appropriate value of the discharge gap, as well as an analytical investigation on the nature of the electrical erosion phenomenon of conductive ceramics.

The developed approach can be extended to newly created composites and nanocomposites with threshold conductivities, and the monitoring system and adaptive control system based on acoustic emission are suitable for any EDM, where the issue of adequate control of processing remains open and unsolved.

2. Materials & methods

2.1. Equipment and materials for development of in-situ monitoring method

The first experiments were conducted on workpieces produced from easy-to-process conductive materials with a low melting point. Workpieces with dimensions of 200 × 20 × 16 mm of sorted and gauged corrosion-resistant, heat-resistant, and high-temperature steel of 12KH18N10T grade (analogue of AISI 321, specifications by interstate standard GOST 5949-75) [83, 84, 85, 86, 87, 88] and 200 × 16 × 16 mm of D16 aluminium alloy (AlCu4Mg1, analogue of AISI 2024) [89, 90, 91, 92, 93, 94] were used.

These experiments were carried out on an industrial 4-axis EDM machine, Seibu M500S (Seibu Electric & Machinery Ltd., Fukuoka, Japan), using a 0.25 mm diameter CuZn35 brass wire with deionised water as medium. The workpieces were fastened at the machine worktable overhang to determine the correlation between the amplitude of the signal and working zone distance. Samples with 2 and 10 mm width were cut off alternately. One single cut was performed for at least five times on each workpiece.

The developed in-situ monitoring system was verified on hard and wear-resistant alloys capable of maintaining their properties at temperatures of 900–1150 °C. The 12 mm long workpieces of hard alloys of VK6O (analogue of M05 by ISO, Table 1) [95, 96, 97] and T15K6 (analogue of P10 by ISO, Table 2) grades [98, 99, 100, 101, 102] were processed on an industrial 4-axis EDM machine AgieCharmilles CUT 1000 (GF Machining Solutions, Bern, Switzerland) using a 0.25 mm diameter brass wire with deionised water as medium. To induce wire tool breakage, the pulse frequencies were changed manually and gradually during processing up to the moment of wire breakage. One single cut was performed for at least five times on each workpiece.

The CNC programs were prepared manually, and the offsets of the path were not taken into consideration. The parameters of the EDM machines were chosen following the recommendations of the manual [103, 104, 105, 106, 107, 108, 109]. The parameters for the first group of experiments are presented in Table 3.

Note that the workpieces were immersed in the dielectric medium for 10 min before processing to exclude the influence of thermal shrinkage of materials during processing [110]. The level of the dielectric medium in the working tank was set as 1–2 mm above the workpieces. The nozzle of the upper guide was set as 2–3 mm higher than the dielectric level.

The experiments were conducted with the use of a pulsed solid-state laser of diode pumping U-15 (RMI, Moscow, Russia) for comparison of the results with those of the monitoring of other impulse precision processes. The laser belongs to the one-mode vanadate laser type Nd:YVO4 with a wavelength $l = 808$ nm [111, 112, 113, 114, 115]. A plate of 200 × 60 × 4 mm of high-quality carbon steel 08 (analogue of AISI 1008, Table 4) was used as a workpiece for laser ablation.

2.2. EDM of conductive ceramics

The 5 mm long × 40 mm diameter samples were produced by the SPS method on a machine for a hybrid current–assisted SPS [116, 117] KCE H-HP D 25-SD (FCT Electronic GmbH, Munich, Germany). The discs were sintered from alumina oxide powder Al_2O_3 with additions of silicon carbide in the form of whiskers SiC_w and 30% of conductive titanium

Table 1
The chemical composition of hard alloy VK6O in %.

Component	WC	TaC	Co
%	92	2	6

Table 2
The chemical composition of hard alloy T15K6 in %.

Component	WC	TiC	Co
%	79	15	6

Table 3
EDM parameters for machining of stainless steel (by the example of SKD-11), which were chosen for experiments.

No.	Designation	Description	Value, equivalent units of machine code
1	V_o	Open voltage, as higher is V_o as faster is processing [code], the high value increase voltage in the discharge gap and instability of processing, in range 30÷150	55÷65
2	V_g	Voltage in the discharge gap for its regulation [code], the high value increase machining speed, decrease the discharge gap and reduce the stability of processing, in range 1÷99	32
3	S_g	Wire feed speed [mm/min]	1÷2
4	C_s	A parameter of high voltage and resistance [code], in absolute values high voltage $V_h = 240$V, resistance $R_o = 8.5\Omega$, standard impulse voltage $V_{imp} = 80$V	101÷102
5	T_o	Time of connection of the current source [code], ~0.1μs in absolute values, in range 1÷15	8
6	T_{off}	Time of disconnection of the current source [code], ~0.1μs in absolute values, in range 6÷50	6
7	T_{hs}	A parameter for T_o [code], in range 11÷99, where '3' is T_{hs} - the second value for T_o for unstable machining, where '4' is T_{hs}' the third value for T_o	43
8	T_{ad}	A parameter for T_{off} [code], in range 104÷550, where "05" is T_{ad} – the second value of T_{off} for unstable machining, "3" is 3·10 = 30 for T_{ad}', when T_{ad} was repeated N times, but unstable machining continues	305
9	S_w	Wire rewinding speed [code], in absolute values ~35 mm/s, 10 min of machining consumes about 20 m of wire; standard brass wire bobbin contains 4.5 kg of wire or about 10500 m of wire; the low value decrease wire vibrations, the high value decrease conical deviation, as wire became finer toward lower guide due to electrical erosion	35
10	F_w	A tension of the tool electrode [code], in absolute values ~3÷4N; the low value leads to larger barrel-shaped deviation for the parts with the external contour and saddle-shaped deviation for the parts with the internal contour, the high value leads to frequent wire breakage	30÷40
11	F_d	A dielectric pressure in nozzles [code], where "2" is high pressure, "45" is a frequency of the pomp 45Hz, the parameter can be regulated on the machine (100÷160, 200÷260)	245
12	N	Switching method between direct and reverse polarity in an unstable cutting mode [code]: switching between T_o-T_{off} and T_{hs}-T_{ad}, the stable cutting is with T_o-T_{off} mode, for the unstable cutting system switches on T_{hs}-T_{ad} mode and then turn back to T_o-T_{off} mode; if it occurs N times, the CNC-system switches constantly for T_{hs}'-T_{ad}' mode (00÷99)	68

Table 4
The chemical composition of carbon steel 08 in % (GOST R standards).

Element	C	Si	Mn	S	P	Cr	Ni	Cu	As	N
%	0.05-0.12	0.17-0.37	0.35-0.65	Up to 0.04	Up to 0.035	Up to 0.10	Up to 0.30	Up to 0.30	Up to 0.08	Up to 0.008

Table 5
Sustainable parameters of SPS assisted by electrical current for production of Al_2O_3-SiCw-TiC conductive ceramic nanocomposite.

Max temperature [°C]	Heating rate [°C·min^{-1}]	Hold time [min]	Maximum pressure [MPa]
1780	100	5	40

carbide TiC in the carbon dies [118, 119]. The control sample was made of tool ceramic VOK-6O (analogue of K01, ISO) [120, 121, 122], which consists of alumina oxide Al_2O_3 and conductive TiC.

The significant difference between the ceramics was in the conditions of production. The first sample was produced in the laboratories of MSTU STANKIN with the maximum achievable homogeneity of powders before hybrid sintering [59]. The main SPS parameters are presented in Table 5 [123,124]. The second sample was produced industrially and was taken from a batch of cutting inserts for lathe machines.

The samples of conductive ceramics were processed by an EDM machine, AgieCharmilles CUT 30P (GF Machining Solutions, Bern, Switzerland). The acoustic parameters of processing were recorded.

A pre-analysis of the specific electrical conductivity of samples showed that their electrical resistance is 40–50 times higher than that of hard alloys. Moreover, the conductivity of ceramics is the minimum possible for materials to be conductors.

A material is considered a conductor if the specific electrical resistance $\rho < 10^{-5}$ Ω m and a dielectric if $\rho > 10^{8}$ Ω m. It should be noted that the electrical resistance of good conductors can be as low as 10^{-8} Ω m, and for the best dielectrics, it can exceed 10^{16} Ω m [125, 126]. Thus, the ceramic samples of VOK-6O and sintered Al_2O_3+SiC_w+TiC can be called conductors with threshold specific electrical resistances, which are suitable for EDM [127, 128, 129, 130].

The value of ρ for conductive ceramics is between the value for graphite of 8.0×10^{-6} Ω m and for nichrome (NiCr) of 1.12×10^{-6} Ω m [131]. A single-crystal graphite is anisotropic with electrical properties close to those of metals along the basic plane of the crystal lattice, when the conductivity in the perpendicular planes is a hundred times less [132]. However, graphite is more conventional in conditions of real manufacturing than NiCr. The EDM parameters for processing ceramics were chosen close to those for processing graphite with the least possible discharge gap. The linear speed of machining was accelerated to trigger short circuiting. The complexity of the work preparation procedures during the experiments is as mentioned above.

2.3. Characterisation of samples

The electrical resistance of samples was measured and controlled using a four-wire connection with a separate power source and a dual-channel nanovoltmeter, Keithley 2182A (Keithley Instruments, Solon, Ohio, USA), according to ASTM C611 standard. The specific electrical resistances ρ of the materials are presented in Table 6.

The microscopy of the samples were analysed by an Olympus BX51M (Ryf AG, Grenchen, Switzerland) microscope with 20k× magnification and a Tescan VEGA3 LMH (Tescan Brno s.r.o., Brno, Czech Republic) scanning electron microscope (SEM) with 1M× magnification.

The spectrometry analysis of the samples was obtained by an X-ray diffractometer using CuKα radiation, PANalytical Empyrean Series 2 (Malvern Panalytical, Almelo, Netherlands). The phase composition was determined using PANalytical High Score Plus software and ICCD-2 database.

A high-precision profilometer, Hommel Tester T8000 (Jenoptik GmbH, Villingen-Schwenningen, Germany), was used to control the roughness of the machined surfaces.

Three-dimensional models and surface profile diagrams were obtained by a certified high-precision 3D microscope, MicroCAD Premium+ (GFMesstechnik GmbH, Teltow, Germany), with an error of ±1 μm.

The cross-sections of the samples for metallography and microscopy were prepared according to the standard probe preparation methods with the use of high-precision equipment: hydraulic press Opal 410, grinding machine Jade 700, and polishing machine Saphir 300 (ATM, Haan, Netherlands).

3. Results

3.1. Development of in-situ monitoring system

The in-situ monitoring system based on vibro-acoustic signals was developed and adopted for the needs of EDM according to the described

Table 6
Specific electrical resistance of the materials ρ with the environmental temperature +20 °C (* given for reference).

No.	Material	Grade	Short chemical description	Analogue (ISO/AISI)	Specific electrical resistance ρ $\left[\frac{\Omega \cdot mm^2}{m}\right]$	Specific electrical resistance ρ [Ω·m]
1	Stainless steel	12Kh18N10T	X10CrNiTi18-10, X6CrNiTi18-10KT	AISI 321	0.746	7.46×10^{-7}
2	Aluminum alloy	D16	AlCu4Mg1	AISI 2024	0.028	2.8×10^{-8}
3	Brass alloy	-	CuZn35, 65/35 brass	ISO 426-1	0.065	6.5×10^{-8}
4	Single-carbide hard alloy	VK6O	WC+Co	ISO M05	0.099	9.9×10^{-8}
5	Two-carbide hard alloy	T15K6	WC+TiC+Co	ISO P10	0.079	7.9×10^{-8}
6	Conductive ceramic of cutting insert	VOK-6O	Al_2O_3+TiC	ISO K01	3.510	3.51×10^{-6}
7	Conductive ceramic nanocomposite sintered in MSTU Stankin [59]	-	Al_2O_3+SiC_w+TiC(30%)	-	3.150	3.15×10^{-6}
8	Nichrome*	-	NiCr	-	1.120	1.12×10^{-6}
9	Graphite*	-	C, 1.CB.05a by Strunz	-	8.000	8.0×10^{-6}
10	Carbide titanium*	-	TiC	-	0.600	6.0×10^{-7}
11	Tungsten*	-	W	-	0.049	4.9×10^{-8}

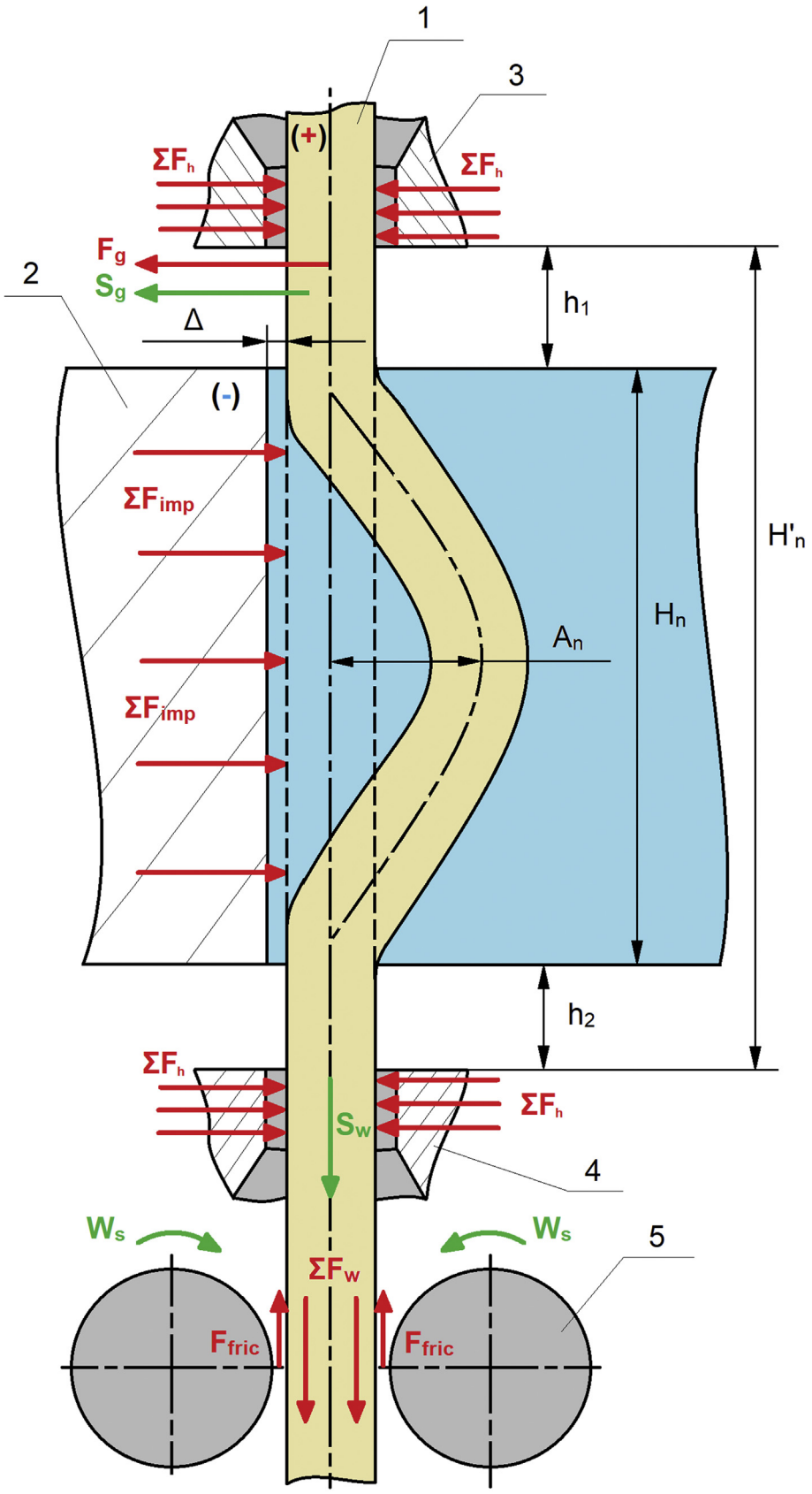

Fig. 3. A diagram of applied forces in the working zone during wire electrical discharge machining: (1) is a wire tool, (2) is a workpiece, (3) is a upper nozzle, (4) is a lower nozzle, (5) is rollers [74].

features below [83, 133, 134, 135].

Investigations [136, 137, 138] showed that the oscillations of the wire tool during processing might be the main reason for instability when the forced oscillations of the wire tool progresses to self-oscillations.

The first experiments showed that the oscillation frequency of the tool in a groove with a substantial thickness of workpiece is close to the frequency established in [139, 140] for mechanical machining.

A diagram of applied forces in the working zone during EDM [141, 142] is depicted in Fig. 3, where

- A_n is the amplitude of the wire in the inverse direction to the wire feed,
- Δ is the discharge gap,
- H_n is the thickness of workpiece,
- H'_n is the distance between nozzles,
- F_g is the force of wire tool guiding,
- ΣF_{imp} is the summation of forces of discharge impact on wire tool,
- ΣF_h is the summation of forces of wire electrode holding in the nozzles,
- ΣF_w is the summation of forces of wire tension and rewinding,
- F_{fric} is the force of friction,
- S_g is the wire feed speed,
- S_w is the wire rewinding speed, and
- W_s is the torsional moment of rewinding rollers.

If the mass of the wire sections between nozzles and the workpiece (h_1 + h_2), which is varied in the range of 3–5 mm (H'_n - H_n), and the mass losses on tool-electrode wear [143, 144, 145, 146] are neglected, then the amplitude of oscillation of the wire tool may be expressed as a complex amplitude of the harmonic signal [147, 148, 149, 150, 151]:

$$\widehat{A}_n = A_0 \cdot e^{\bar{\beta}\tau}, \tag{1}$$

where A_0 is the amplitude in the direction of wire feed, which is limited by the discharge gap Δ and is less than Δ, $A_n \leq A_0$ for stable EDM, $\bar{\beta}$ is the damping coefficient expressed as a complex number in the form $a + bi$, and τ is the period of oscillation T.

$$\bar{\beta} = \bar{q} - \bar{\mu}, \tag{2}$$

where $\bar{q}$ is the index of excited oscillations (a complex number), and $\bar{\mu}$ is the coefficient of dielectric medium resistance. In this case, $\bar{q}$ is

$$\bar{q} = \sqrt{\frac{\sqrt{h} - \bar{k}}{2 \cdot m_n}}, \tag{3}$$

where h is the ratio between H_n and H_0:

$$h = \frac{H_n}{H_o}. \tag{4}$$

H_0 is the critical value of workpiece thickness, which is a characteristic of stable EDM to guarantee sufficient quality and geometric accuracy of the processed surfaces. H_0 = 80–100 mm is the commonly known industrial recommendation for a wire diameter d_w = 0.25 mm and a water-based dielectric medium, whereas H_0 = 8–10 mm for conductive ceramics. m_n is the mass of wire on the length H_n, while $\bar{k}$ is a complex number of the ratio between K_0 and K_n:

$$\bar{k} = \frac{K_n}{K_0}. \tag{5}$$

Here, K_n is the stiffness of the system, and K_0 is the stiffness of the system for stable EDM. For a particular case, K_n can be expressed as

$$K_n = \frac{\sum F_{imp}}{A_n}. \tag{6}$$

The coefficient of dielectric medium resistance $\bar{\mu}$ [kg/s] is approximately correlated and inverse directed to F_{imp}. Hence, $\bar{\mu}$ depends on the density of the dielectric medium ς, strength area Π_s, and wire feed speed S_g. It can be expressed as

$$\bar{\mu} \approx -\sum \overline{F_{imp}} = \left|\varsigma \cdot \Pi_s \cdot S_g\right| = \left|\varsigma \cdot \pi \frac{d_w \cdot H_n}{2} S_g\right|. \tag{7}$$

Thus, β depends on the ratio between the workpiece thickness and stiffness of the system, the process parameters, and viscosity of the working medium in the groove; it can vary in the limits of |1|.

A criterion for the self-oscillation process origin is

$$q = \frac{\lambda}{T}, \tag{8}$$

where λ is the logarithmic decrement characterising the damping ratio of self-oscillation and, as a rule, is a resonant process describing the decrease in the amplitude of the oscillation process. It is equal to the natural logarithm of the ratio of two successive amplitudes of an oscillating quantity A_n at the same side:

$$\lambda = ln \frac{A_n}{A_{n+1}}. \tag{9}$$

The period of self-oscillations T depends on the mass of the wire on the length H_n and stiffness of the system, which depends on the wire tension:

$$T = 2\pi \sqrt{\frac{m_n}{K_n}}. \tag{10}$$

If $|q| < |\mu|$, then self-oscillations (including resonant) do not occur. If $|q| > |\mu|$, then self-oscillations are generated, and the higher the intensity, the higher the excess of $|q|$ over $|\mu|$.

Note that μ is higher for an oil medium and lower for a dielectric medium based on water. Thus, EDM in an oil medium gives a better geometric accuracy in processing critical surfaces of parts with thickness of the workpiece larger than 80–100 mm for conventional conductive materials and larger than 8–10 mm for conductive ceramics.

The developed in-situ monitoring system [74] consists of accelerometers (which were placed at the upper guide and fastening system), preamplifiers and amplifiers (VShV003, Moscow, Russia), an analogue–digital converter (E440, Moscow, Russia), and a signal-recording device. The signals received from the accelerometers depend on the nature and intensity of the vibrations during processing, which depend on the summation of forces of discharges ΣF_{imp} that rely on the EDM parameters.

The first experiments showed that the upper accelerometer gave a more informative symmetric signal than the lower one. Further, only the signal from the upper guide was considered. The vibro-acoustic signals were recorded with the following intervals: 1 min, 30 s, and 5 s before the end of processing. A spectral analysis was conducted for frequencies up to 10 kHz.

3.2. Validation of the developed system on conductive ceramics

The features of oscillation signals during conventional metalworking are relatively well-known [152, 153, 154, 155]. The recent studies completed this knowledge with the data concerning the control of electric discharge based on electromagnetic and vibro-acoustic emissions [156, 157, 158, 159, 160]. Further studies of the signal features during EDM of conductive materials showed a particular behaviour of the signal, which is suitable for the development of the monitoring method [75, 133, 134]. The developed adaptive control system based on acoustic emission could function along with a system based on electrical parameters, or even replace it totally. The obtained results demonstrated that vibration monitoring might provide relevant data about the state of

processing. It may prove to be essential for controlling more complex machining processes for new classes of materials such as conductive ceramic nanocomposites. Thus, two types of conductive oxide ceramics were selected:

- a 5 mm long × 40 mm diameter cylindrical sample of sintered ceramic nanocomposite Al_2O_3+SiC_w+TiC with 30% of TiC for providing better electrical conductivity, and
- a 5 mm long square cutting insert for a lathe machine tool made of a conductive tool ceramic Al_2O_3+TiC grade of VOK-6O (analogue of K01 by ISO).

Fig. 4 presents a portion of records of the root-mean-square (RMS) values of vibration and current signals during the EDM of Al_2O_3+SiC_w+TiC ceramic. Note that the peaks and dips of the signals are opposed as marked by arrows.

Short circuiting is associated with the dips of the vibration signal and sharp rises of the working current signal. The high electrical resistance of the conductive ceramics provided moderate alterations of the voltage and current during short circuiting. It did not permit determining these changes by the CNC system and applying timely corrections of the EDM parameters.

Studies [161, 162] showed that the growth of energy and efficiency of pulse acting on the surface to be machined is followed by a gradual increase in the RMS amplitude of vibration signal at a high-frequency band.

In the beginning, the segment of the wire probably was overheated and partly melted, and a subsequent breakage followed. At the same time, the wire rewinding rate was sufficient and adequate to continue processing. The observed quality of the machined surface was not sufficient because of the conducted experiments on optimization of EDM parameters during machining.

Fig. 5 presents the roughness of the machined surface, where R_{max} at a length of 1.0 mm is more than 65 μm.

The process of EDM of the sample made of VOK-6O conductive ceramic was also forced to have frequent short circuits. The received record of VOK-6O sample processing shows similar slumps of the RMS amplitude of the signal at the moment of growth of the discharge current.

Fig. 6 shows the RMS values of vibro-acoustic signals in the octave band of 16 kHz and current signals. The lowest values of vibration signals are recorded at 0.35 s of short circuit when the highest peaks of the working current were observed. At the moment of short circuits, the vibration signal had a significantly different spectrum characteristic than during the stable phase of machining. This type of spectrum is associated with frictional contact [163, 164, 165, 166, 167].

Fig. 7 depicts the spectra of vibration signals recorded during the stable EDM and at the moment of short circuits. The amplitude of the vibro-acoustic signals during the stable EDM was many times higher than that during short circuits. The characteristic of the signal during short circuits was similar to that of the signal during stable EDM, which could be due to the electrodes' physical contact and friction. It is especially visible in the areas of spectral peaks associated with own frequencies of the 'tool with guide nozzles–workpiece with fastening elements–machine' system. During the detected friction contact, the vibro-acoustic amplitude was low and primarily defined by the speed of the relative movement of electrode surfaces and their hardness [137, 168, 169]. The wire rewinding speed was approximately 150 mm/s. The characteristic of the amplitude was different from that of the signal related to the work of the pump and EDM machine drivers. This can be helpful in detecting the moment of contact loss between electrodes during the reversal motion of the guides when the pulse generator is switched off. In other words, the CNC system should immediately dispatch a signal to switch the pulse generator off and switch the reverse mode on to break the contact between electrodes. Afterwards, the wire tool should be re-approached and the generator switched on.

4. Discussion

4.1. Nature of oscillations during EDM

In the beginning, it was decided to focus on the moment of the part separation from the workpiece. Changes in the specific noise accompanied the process—from the monotonic buzzing sound to the higher-pitched sound gradually ascending to the moment of brittle fracture.

The experiments showed that the amplitude of the vibro-acoustic signals increases gradually when approaching the moment of part separation from the workpiece. Then, a series of characteristic peaks of the vibro-acoustic signals is observed. It provides an indication about the final bridge weakening between the part and workpiece. It slowly starts the motion under its mass accompanied by the discharge current pulses. The recorded signal demonstrates plastic and brittle stages of bridge rupture [10, 11, 29] at that moment. Additionally, the wire tool can be squeezed between the part and workpiece, and a series of short circuits, which causes the formation of burn defects at the machined surface [28], occurs.

During the experiments, it was established that even negligible changes in the part weight are reflected in the vibro-acoustic signals. For example, a 24.5 g weight and a 10 mm width sample of stainless steel show instability, which was recorded by a significant increase in the amplitude of the vibro-acoustic signals 5 s before separation. In addition, a 4.28 g weight and a 10 mm width sample of aluminium alloy show the beginning of separation moment, i.e. plastic deformation, which leads to wire tool clasping during the final bridge rupture 2 s before separation. This phenomenon was recorded in the broad frequency range of the signal and was also characterised by instability in the low frequencies. Thus, it was decided to use a frequency range higher than 4 kHz for monitoring and further analysis.

Note that the effective amplitude in the octave-frequency band is more stable than the high-frequency spectra of the vibro-acoustic signals

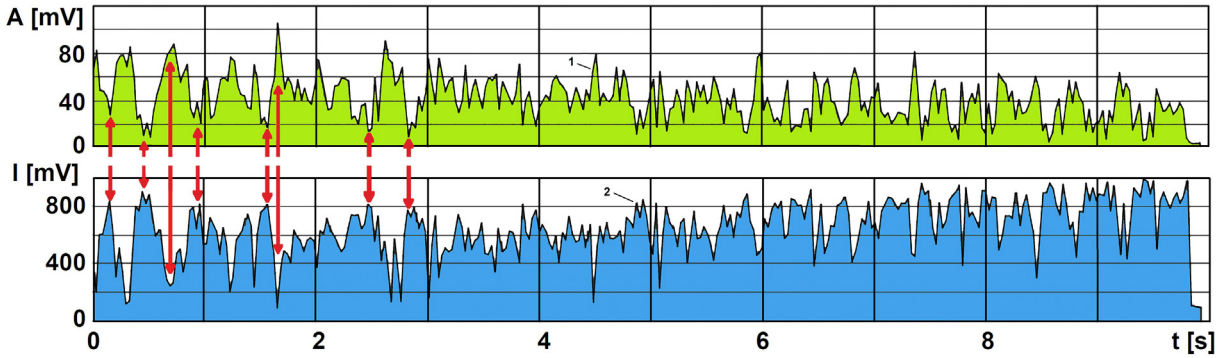

Fig. 4. RMS diagrams during wire electrical discharge machining of the sample made of Al_2O_3+SiC_w+TiC nanocomposite: (1) is the recorded vibroacoustic signal; (2) is the recorded operational current.

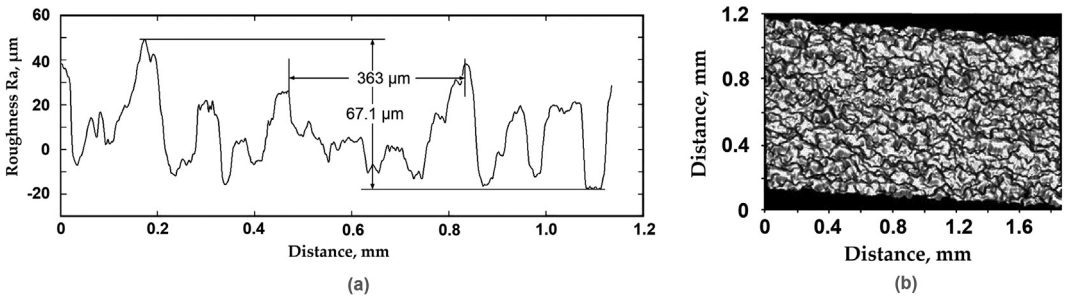

Fig. 5. The machined surface of the sample made of Al_2O_3+SiC_w+TiC nanocomposite after WEDM: (a) is microrelief of the surface; (b) is three-dimensional surface profile in the upper corner.

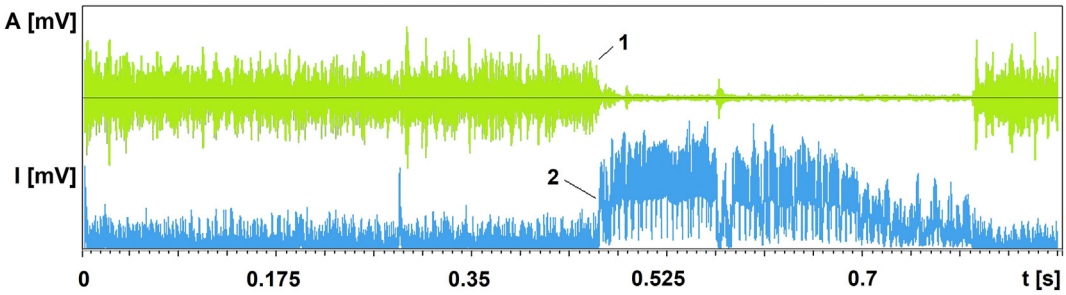

Fig. 6. RMS diagrams at the moment of the short circuit during WEDM of the sample made of VOK-6O conductive ceramic composite: (1) is the recorded vibroacoustic signal; (2) is the recorded operational current.

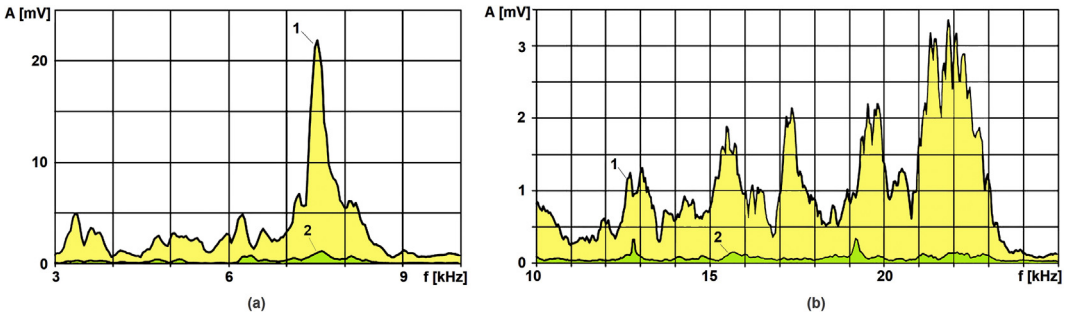

Fig. 7. Spectra of the vibroacoustic signal during WEDM of the sample made of VOK-6O conductive ceramic composite: (a) is in the low frequency range; (b) is in the high frequency range; (1) is for regular processing; (2) is for short-circuit.

because of averaging by the wider frequency range. As the moment of rupture approaches, the effective amplitude increases by approximately two times in the octave-frequency band of 4 kHz and, at the same time, the effective amplitude increases by 1.5 times in the octave-frequency band of 8 kHz [74]. According to these changes in amplitude, the processing state can be evaluated without access to the working area and by visual demonstration, which can be understood even for the inexperienced operator and used for adaptive control.

During the final rupture of the part from the workpiece when under the influence of its weight and discharge current pulses, the part starts its movement relative to the workpiece due to the natural process, which is similar to the stress–strain curve for construction materials [170, 171, 172], and the signal was recorded (Fig. 8). The movement disturbs the symmetry of the wire tool position in the formed groove, alters the discharge gap, and the subsequent contact of the wire tool and workpiece occurs inevitably.

It was detected that separate components of the spectrum on the last seconds of the records increase by ~4 times in the frequency band of 8 kHz for aluminium alloy. The described changes in the vibro-acoustic signals are sufficient for developing the in-situ monitoring system and system of adaptive control to prevent undesirable short circuits and increase quality of the machined surfaces.

As it was determined, an excess in the amplitude of the vibro-acoustic signals shows the instability of the discharge gap Δ, which can be explained by the presence of erosion products in the discharge groove. It gives a basis for interactive changes in the EDM parameters during processing (adaptive control) especially at the moments of wire penetration and at the end of the operation to decrease the disturbing influences on the wire tool. The stability of the vibro-acoustic signals occurs when the discharge current pulses are uniformly distributed over time, the processing area of the workpiece is less than 70–100 mm thickness, and a sufficient, timely flushing of the erosion products from the discharge gap is ensured.

The influence of the wire tool tension force F_w on the vibro-acoustic signals during the experiments was evaluated by varying its range at ± 0.5 N (~5 equivalent units of machine code). On the spectra of the vibro-acoustic signals' parameter records, on the length of stable machining of 12Kh18N10T stainless steel samples with a wire force tension F_w at a value of 3 and 4 N, there is an RMS signal dispersion with time (Fig. 9). However, with the decrease in tension, the tendency towards absolute

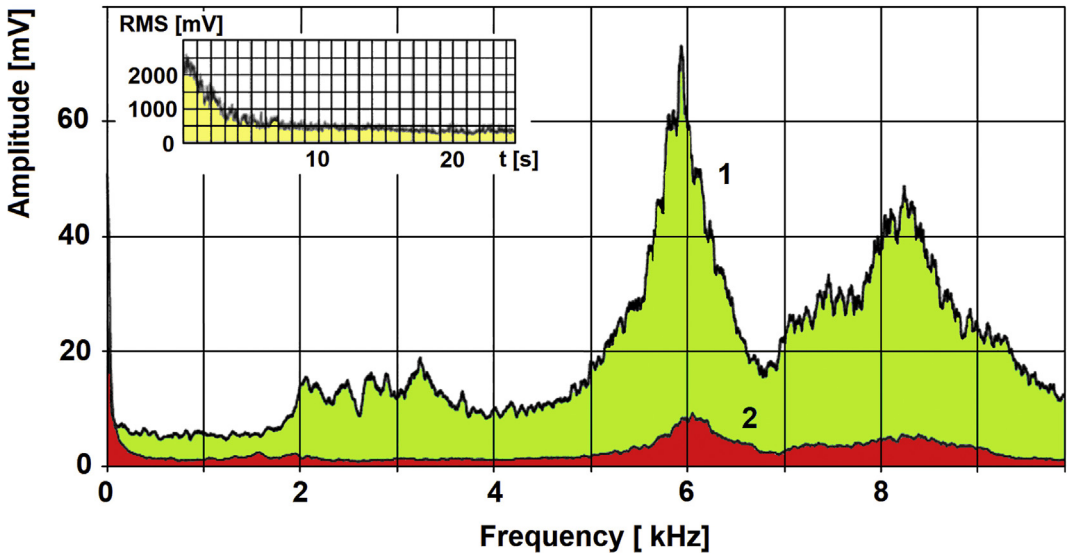

Fig. 8. High-frequency spectra of the vibroacoustic signals during WEDM of the samples made of D16 aluminum alloy: (1) is at the moment of wire tool penetration; (2) at the moment when the discharge gap Δ is formed; the inset of RMS-t diagram presents the spectrum of the vibroacoustic signal at the moment of wire tool penetration.

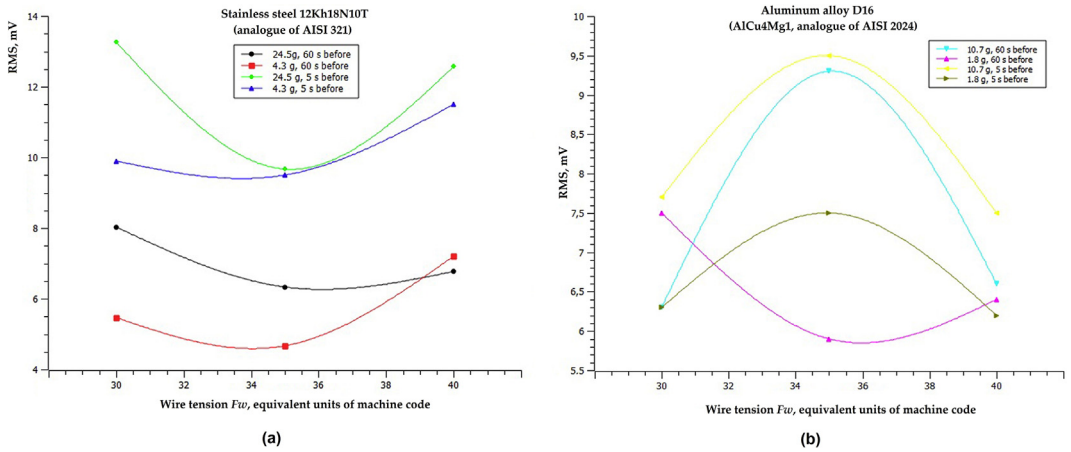

Fig. 9. RMS of octave spectra at the frequency band of 8 kHz with a variation of wire tension $F_w \pm 5$N from the value of wire tension of stable WEDM: (a) for samples made of 12Kh18N10T stainless steel; (b) for samples made of D16 aluminum alloy.

values of parameters is traced for the range of high frequencies. The variation of F_w has a similar tendency for stainless-steel samples at 5 and 60 s before the end of processing (Fig. 9a). The characteristics of the diagrams for the two types of materials are different. This can be explained by the different elastic properties of the materials (Young's modulus): the higher the elasticity of the system, the higher the sensitivity of the developed monitoring system (Fig. 9b). A decrease in the stiffness of the technological system components obstructs oscillation propagation [173, 174, 175, 176, 177]. It can be an advantage in the application of the developed system for processing of materials with

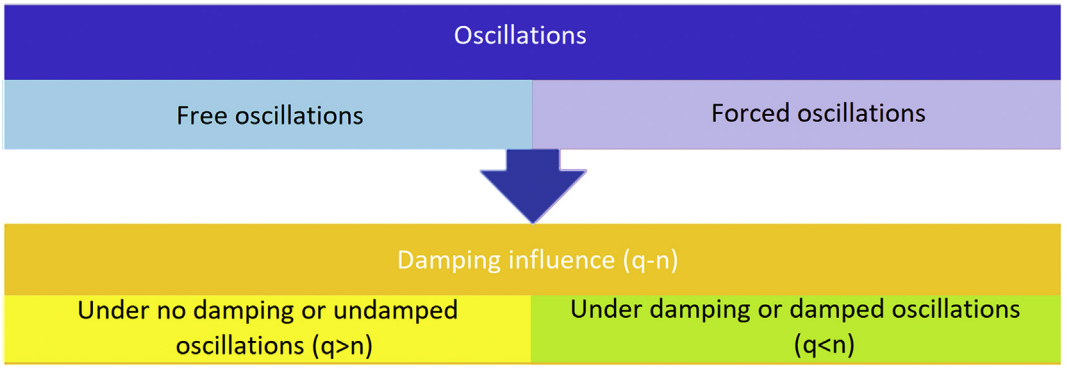

Fig. 10. The types of oscillation.

advanced mechanical properties such as conductive ceramic composites and nanocomposites.

Note that the RMS value of amplitude at 5 s before the end of processing exceeds the RMS value of amplitude at 60 s before the end of processing by at least 2 times at the frequency band of 8 kHz. The difference in RMS values decreases as the wire tension grows, demonstrating the lesser dependence on the weights of the samples, which differ by ~6 times, as the stiffness of the system grows.

As it is known, there are three types of vibrations in technological systems (Fig. 10):

1. Free natural oscillations, which are characterised by a specific frequency ω_{nat} determined by the properties of the technological system.
2. Forced oscillations, which are characterised by a periodically acting external force F_{imp}, in the case of EDM. The frequency ω_{frc} is determined by the frequency of discharge impulses, and the amplitude is related to the resonance phenomenon.
3. Self-oscillations, which are characterised by the internal energy of the system with a fixed frequency ω_{slf} close to the frequency of natural oscillations ω_{nat} and a fixed amplitude. They are associated with the low stiffness of the system and fluctuation of the acting force F_{imp}. The frequency of vibrations increases with an increase in the system stiffness and decreases with a decrease in the workpiece thickness.

Because low-frequency vibrations (10–100 Hz) are associated with the appearance of low-frequency noise related to the work of the equipment and guiding bars and high-frequency oscillations (1500–8000 Hz) are associated with the wire tool vibrations and high-frequency noise (close to whistle) accompanying processing, it is recommended that EDM takes place outside the specified zone to exclude the phenomenon of resonance [178]:

$$0.7 < \frac{\omega_{frc}}{\omega_{slf}} < 1.3. \tag{11}$$

Then, the process may be characterised as a process of stable cutting. Three groups of forced oscillations can be distinguished during EDM:

1) Oscillations associated with the frequency characteristic of the electric current pulses discharged on the surface to be machined. The wire tool has larger oscillation amplitudes due to its lower stiffness and mass.
2) Oscillations caused by the design features of the EDM machine and drives of its guides.
3) Any other external oscillations.

Thus, based on the items mentioned above, we can conclude that

- For the lower value of wire tension, flushing of the erosion products is hampered by wire bending and its higher amplitude due to the low frequency of vibrations, which have a complex characteristic, when ω_{frc} is greater than ω_{slf}.
- For the higher value of wire tension, flushing of the erosion products is adequate, but the stiffness of the system is higher. Moreover, the wire amplitude is lower and the vibration frequency grows when ω_{frc} is less than ω_{slf}.
- For the value of wire tension associated with stable cutting, the frequency of forced oscillation ω_{frc} may be compensated by the frequency of self-oscillation ω_{slf}.

During the disturbance of stable machining in the initial motion of the separating part, the influence of the vibro-acoustic signal parameters is less noticeable than that at the end of the operation. It may be explained by the phenomenon when the additional forced disturbances defined by part mobility mainly influence the increase in vibro-acoustic signal amplitude.

4.2. Productivity of pulses and origin of instability during EDM of conductive ceramics

The optimisation of EDM aims to ensure its maximum productivity, efficiency, and surface quality. This demands the maintenance of constant conditions or the regulation of process parameters, such as the discharge gap Δ, the concentration of erosion products in the gap, the temperature of the working fluid, and its flow rate. The gap Δ is the main parameter as it is mostly responsible for determining the quality of EDM, which occurs within the discharge gap [179, 180]. A small increase in Δ may change the breakdown conditions or even interrupt the discharge; a decrease in Δ impairs the yield of erosion products, reduces the productivity, promotes slag buildup on the electrodes, and facilitates short circuits. Without automatic regulation of the gap, EDM is ineffective [1, 12, 72]. For better regulation, Δ must be maintained above the value at which short circuits appear, and below the value at which breakdown is impossible and idling pulses appear. In maintaining an optimal gap, the rate of particle formation M_p in the discharge gap has to be equal to the rate M_{ex} at which the particles (debris) leave the gap. The rate M_p is a function of the particle concentration γ:

$$M_p = f(\gamma). \tag{12}$$

When M_p and M_{ex} are unequal, the change in concentration is

$$\Delta\gamma = \Delta M \frac{\Delta t}{Q}, \tag{13}$$

where Q is the volume of the discharge gap and

$$\Delta M = M_p - M_{ex}. \tag{14}$$

For stable processing,

$$\Delta\gamma = 0. \tag{15}$$

However, it is complicated to ensure a constant γ due to the many random factors that act on the working zone [181]. Any fluctuations that arise must be promptly eliminated by control signals that change the EDM parameters through diagnostic information. Fig. 11 shows the dependence of the rate M_p on the discharge gap Δ with different exit rates of the particles:

$$M_{ex1} > M_{ex2} > M_{ex3}. \tag{16}$$

Analysis indicates that the maximum machining rate M_p decreases as

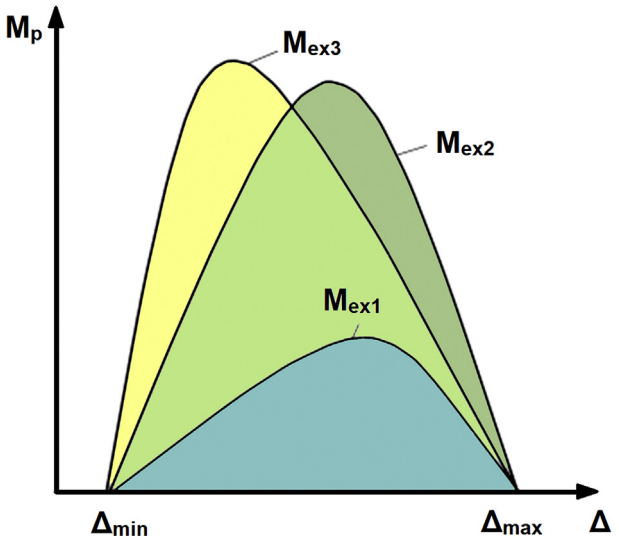

Fig. 11. Dependence of the rate of particle formation M_p on the discharge gap Δ at various exit rates M_{ex} of the erosion products.

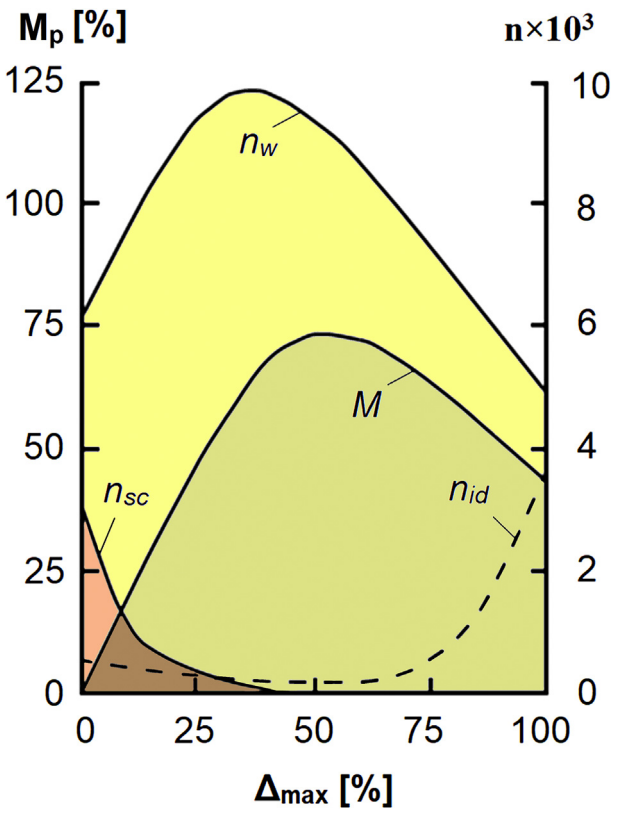

Fig. 12. Dependence of the rate M_p and the number of pulses n on the discharge gap Δ [74].

M_{ex} reduces because of the deterioration in the discharge of erosion products as the electrode is introduced in the material, and the number of working pulses is reduced [182, 183, 184].

Fig. 12 illustrates the dependences of the machining rate M_p, number of working pulses n_w, number of idling pulses n_{id}, and number of short circuit pulses n_{sc} on the discharge gap Δ. Analysis shows that the gap corresponding to the maximum machining rate M_{max} is higher than the gap corresponding to the maximum working pulses ($n_{w.max}$). It may be explained by the excess of erosion products at $n_{w.max}$ and the presence of short circuit pulses, which destabilise the process [133, 134, 185, 186].

Therefore, the in-situ monitoring and control systems aim to maintain the efficiency of pulse utilisation in the range of

$$\psi_{pu} = 0.7\text{–}0.9. \tag{17}$$

It may be calculated as the ratio of the number of working pulses n_w that are involved in the process of material ablation to the total number n of pulses:

$$\psi_{pu} = \frac{n_w}{n}. \tag{18}$$

While ψ_{pu} is useful for in-situ adaptive control, its use is hindered by the complexity and inertia of the measuring instruments required. Besides, it is difficult to assess the efficiency of EDM with respect to ψ_{pu} [161, 187]. When the working fluid is contaminated with erosion products, the energy of the individual pulses is not entirely consumed in the process of metal ablation; some of the energy is consumed in the destruction of the erosion products [188, 189, 190]. Thus, the number of working pulses is assessed from the total width of the discharge pulses or their height at the front and back of their profiles. It leads to an imprecise assessment of the efficiency of EDM.

A more precise estimate may be obtained by relating the efficiency to the ratio of the useful energy consumed in the destruction of material and the total energy that enters the working zone in the form of discharge pulses. In the operation of independent generators, the energy of the discharges is proportional to the effective discharge current (I_e). A current sensor may be used to estimate this energy.

The parameters of the vibro-acoustic signals recorded by the accelerometer mounted on the workpiece were used to assess the useful energy. Monitoring based on acoustic emission is used for tool assessment in conventional machining processes [72, 73]. However, the widespread use of vibro-acoustic signals for in-situ monitoring of cutting and friction is difficult because a closed system with a nonlinear dependence of the vibro-acoustic signal on the contact load is formed with the direct contact of the tool and workpiece or contact of the indenter and counter body [152, 153, 191, 192, 193]. This nonlinear dependence is not observed when energy pulses act on the workpiece. Hence, the dynamic system resembles a linear model better, where the dynamic relation between the load source and the workpiece is permanent. In other words, the model of the dynamic system is significantly simplified, and its use in the in-situ monitoring and regulation of machining by high-energy fluxes is simplified [168, 189, 194, 195].

Let us consider the results of vibro-acoustic monitoring of another non-contact precise machining method, which allows the processing of materials for industrial manufacturing applications (micromachining, laser graving, and grinding). Laser treatment is close by its nature to the processes of material removal during EDM because in both cases, there is no mechanical contact between the 'tool' and workpiece [196]: the material removal occurs under thermal influences, initiated by pulses of concentrated energy flows. The mechanism of material removal during EDM is related to the processes of sublimation or evaporation [180, 197, 198, 199, 200, 201], similar to the mechanism of material removal during laser treatment, which is also called laser ablation [202].

The previously conducted experiments using a pulsed solid-state laser of diode pumping have shown that the vibro-acoustic signals during the processing of a workpiece made of high-quality carbon steel 08 (analogue of AISI 1008) steadily rise as the laser power rises and the volume of removed material increases [133]. The amplitude of vibro-acoustic signal A depends on the power of the impulses, and the experimental dependence of productivity of single pulses is directly proportional to their power. Therefore, the monitoring of vibration signals can be recorded or evaluated visibly and timely in contrast to the evaluation of the abstract concept of current pulses productivity.

Based on data published in [74, 133, 203], it can be concluded that there is a direct dependence between the discharge productivity of pulses and the usable energy proportion, and an inverse dependence with the duration of pulses. In the case of machining of materials with low or threshold conductivities such as conductive ceramic composites and nanocomposites, the duration of pulses will be so small such that it can be ignored in the calculations. Therefore, the main reason for EDM instability when the value of the workpiece thickness H_n is less than the critical value H_0 ($H_n < H_0$), which characterises stable EDM processing, can be the strong correlation between the usable energy proportion and concentration of erosion products in the channel of observation. When $H_n > H_0$, there should be at least two main reasons of process instability: the concentration of particles in the volume of the discharge gap Q, which is dependent on the main technological parameters, and self-oscillations of the wire, when the stiffness of the system K_n is less than the critical value K_0.

A dynamic model of the concentration of erosion products and its influence on the vibro-acoustic signal parameters was presented in previous works [74, 203]. It was shown that although EDM is a non-contact processing method, the developed technique of diagnostics based on vibro-acoustic signals may be used as a reliable in-situ monitoring system as in the case of many other processing methods based on mechanical contact between two components [152, 194, 204, 205, 206, 207, 208, 209].

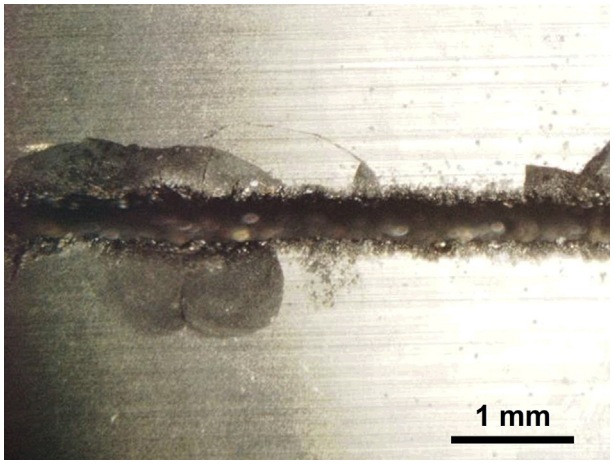

Fig. 13. A picture of the machined groove of the sample made of VOK-6O conductive ceramic composite after WEDM accompanied by series of short circuits.

4.3. Electrical erosion phenomenon of conductive ceramic composites and nanocomposites

A similar graph of vibro-acoustic signals was obtained during EDM of the samples made of VOK-6O. The vibro-acoustic signal related to the short circuits was accompanied by the indicated presence of frictional contact between the electrodes under voltage. As a result, the machined surfaces have traces and defects associated with the formation and development of brittle cracks related to excessive heating in the working zone. Fig. 13 shows a photograph of the sample made of VOK-6O conductive ceramic, where the mechanical destruction of the edges around the formed groove of the workpiece can be found. The formed cracks cause chipping of the ceramic sample, with the debris size exceeding the width of the groove of ~0.26 mm in a few times. It was detected that the formed brass globules condensed on the machined surfaces of the groove during short circuits. This could be due to the inappropriate combination of materials for the wire tool and workpiece. The melting and boiling points of the components of these materials differ significantly. In this case, the melting and boiling points can be used as references for estimating the initiation temperature of the sublimation phenomena.

According to study results [169, 210, 211], sublimation of brass under vacuum conditions starts with zinc as the most fusible material at 450 °C (the melting point of zinc is 419.5 °C, whereas the melting point of copper is 1085 °C). At the same time, a nanoporous structure is formed in the remaining copper [169]. The studies showed that when brass sublimates under normal conditions in the presence of an air medium, a whitish needle-shaped film forms for zinc oxides at a temperature of ~300 °C, a single-layer film of CuO at a temperature of 300–375 °C, a bilayer film of black CuO, and a dark red Cu_2O at 375–1100 °C.

The absence of traces of oxide films on the surface of the wire after EDM (Fig. 14) indicates that the conditions of the formed discharge channel are close to the conditions of brass sublimation in a vacuum. That is, an active medium of interaction with materials is absent. The presence of C and Si in Fig. 14b can be explained by the use of epoxy resin for filling the probe of the sample for the analyses.

Therefore, with a discharge channel, the conditions in the inter-electrode gap are similar to the conditions of laser sublimation in a vacuum. However, it differs in the thermal source: it is the breakdown spark during EDM that initiates the occurrence of a conducting discharge channel. Hence, the sublimation, which begins with zinc, with increasing temperature progresses to the sublimation of copper. By the time the temperature reaches the critical value for the initiation of sublimation of alumina in the inter-electrode space, a relatively dense gas medium is formed. It leads to the formation of a plasma cloud (a rapidly expanding low-temperature plasma cloud) and prevents further sublimation. The surface of the electrodes partially adsorbs the gaseous material of the plasma, which also prevents continued sublimation. The results of the SEM of samples made of Al_2O_3+TiC(30%) conductive ceramic with similar conductive properties as the Al_2O_3+SiC_w+TiC(30%) sample produced by the SPS method assisted by electric current (Fig. 15) show a picture of the distribution of the chemical elements before and after EDM. Fig. 15b illustrates the chaotically distributed components of the wire electrode and workpiece on the machined surface of the ceramic. The X-ray spectrometry analysis of VOK-6O conductive ceramic (Fig. 16) can also corroborate the above-mentioned assumption.

Thus, the temperature in the inter-electrode gap reaches that of TiC sublimation with the melting point of ~3140 °C. However, the formed gas phase of alumina, zinc, and copper adsorbed by the surface of the nanoporous structure of titanium carbide prevents the removal of material in sufficient volume (efficient mass loss) at the formed groove. Then, the spark is re-initiated, and the cycle repeats.

The nanoporous structure (the recast layer + heat-affected zone) after sublimation occurs at a depth of 15–20 μm with a pore size of 2 ± 1 μm according to Mahdavinejad [170], Kazanskiy [210], and Ren [211]. In the conducted experiments with EDM, it can be said that the defects of the machined surface with a change in its chemical composition are determined to a depth of up to 4 μm [10, 11, 29].

The multiple cases of short circuits can be explained by the fact that the electrical resistance of the workpiece material is approximately 100 times higher than that of efficiently processed materials such as aluminium, steel, and hard alloys. These materials have different corresponding values of discharge gaps.

Thus, it can be assumed that during EDM of conductive ceramics, contact between the electrodes in the spark gap occurs due to a significant loss in the wire material with a sufficiently long pulse. The machining proceeds according to the scenario described above, when the easy-to-melt components of the wire electrode settle on the structure formed from the refractory titanium carbide. The wire continues rewinding and renews uninterruptedly the electrode material at the inter-electrode gap and feeds forward. At a particular moment, the wire material on the surface of the workpiece accumulates such an amount that provides partial adhesion of the electrodes in the spark gap. There is constant contact between the electrodes due to the filling of the inter-electrode space with the products of erosion, leading to short circuits without the possibility of having the wire off from the workpiece to re-establish the spark gap. Consequently, the wire electrode breaks due to the impossibility of further rewinding and the CNC system of the machine gives a signal on the interruption of processing and shows an error code in the display.

It should be noted that the current monitoring of the conditions in the inter-electrode space based on the electrical parameters remains blind to the processes happening between the two electrodes before wire breakage. This leads to defects in the machined surfaces and machining interruptions.

4.4. Discharge gap and wire tool material for EDM of conductive ceramics

The experimentally determined value of the spark gap for conductive ceramics was in the order of 0.005 mm, which is 15 times less than the recommended value for aluminium alloys of 0.075 mm. The value of 0.005 mm is more difficult to control by the drives of the EDM machine with a positioning accuracy of 2–3 μm; environmental conditions may also affect the accuracy of processing at rough modes. It should be noted that the difficulties in slot forming are related to the inappropriate combination of electrode materials and insufficient space for wire oscillations under pulses.

During the EDM of VOK-6O conductive ceramic, slender metallic fibres were formed on the globules of easy-to-melt components of the wire after short circuiting and at the moment of contact loss between the

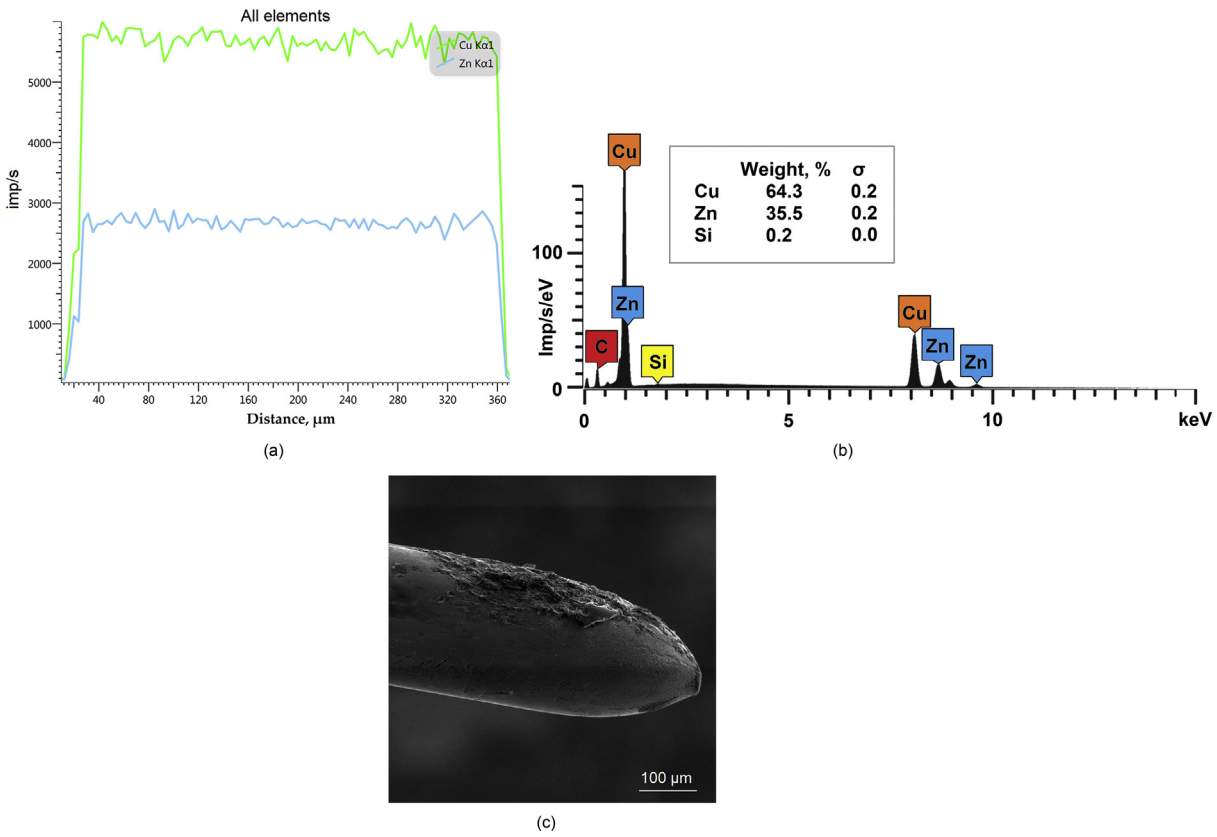

Fig. 14. Characterization of wire tool after WEDM of the sample made of VOK-6O conductive ceramic composite: (a) distribution of all chemical elements along the diameter; (b) X-ray spectrometry analysis; (c) SEM of the wire tool break point with the presence of the erosion traces.

electrodes. These fibres continue to keep the contact between the electrodes at the reverse motion of the wire for re-establishing the discharge gap and prevent further processing.

Fig. 17 shows a picture of the formed groove, where solidified globules and fibres of 6–10 μm in diameter can be observed.

The TiC content in the samples made them conductive because the electrical resistance of titanium carbide is 6.0×10^{-7} Ω m [212, 213], which is higher than that of CuZn35 brass. However, the temperature stability field of TiC reaches 3140 °C, which is highly resistant to molten low-melting metals and metals such as copper, aluminium, brass, cast iron, and steels [214, 215]. The primary component of the matrix is alumina, which is known as an excellent dielectric [216, 217], but some researchers consider it an n-type semiconductor with a permittivity of 9.5–10.0 and an electric strength of 10 kV/mm [218]. The melting point of aluminium oxide is 2044 °C, whereas the boiling point is 2977 °C [219, 220, 221, 222]. Note that the boiling point of any alloy depends on its components. The first component of the brass wire that reaches the boiling point of 907 °C is zinc; next is copper with the boiling point of

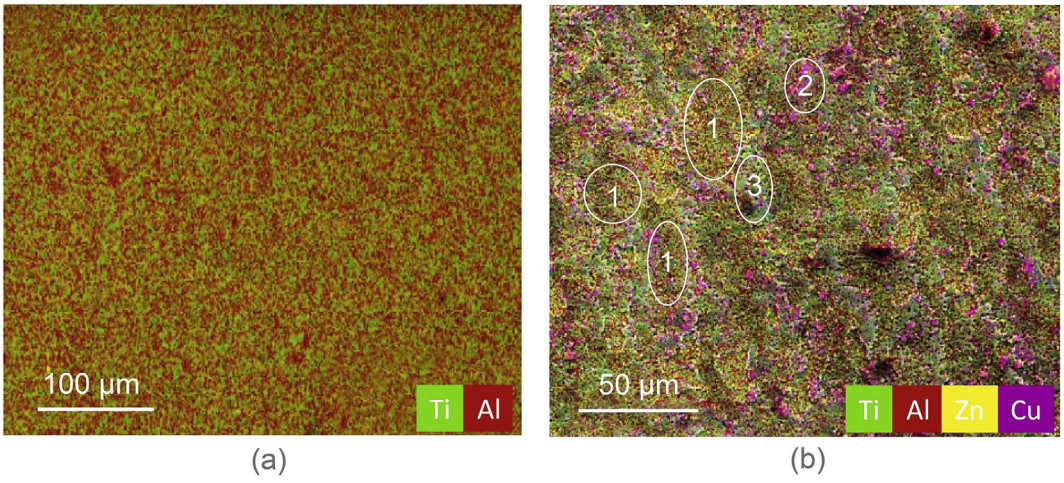

Fig. 15. SEM analysis of the chemical elements distribution of the samples made of Al_2O_3+TiC(30%) conductive ceramic nanocomposite: (a) cross-section of the sample before WEDM; (b) machined surface after WEDM, where (1) is nanoporous structure of the main components of the sample, (2) and (3) adsorbed easy-to-melt components of the wire tool.

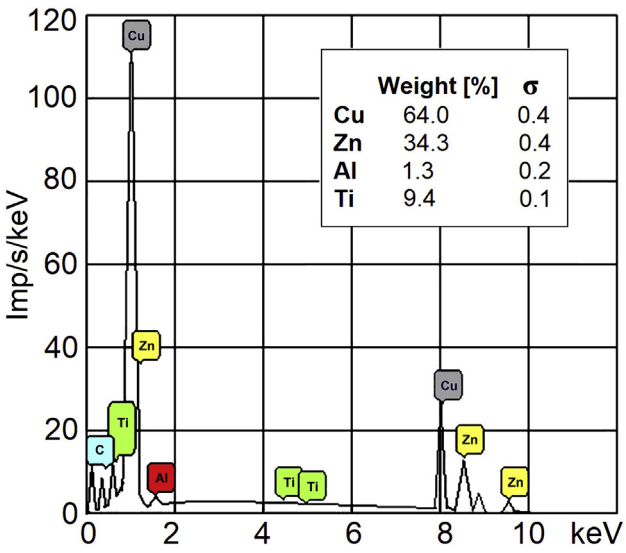

Fig. 16. X-ray spectrometry analysis of the machined surface of the sample made of VOK-6O conductive ceramic composite after WEDM.

of machined surface quality and performance during conventional EDM. The method can be adopted for

- workpieces with large thicknesses (more than 150–200 mm),
- workpieces with a remotely placed working zone (more than 100 mm from a nozzle),
- workpieces with uneven internal structures such as a set of hollow tubes, and
- workpieces made of materials with threshold conductivities and high heat resistances (heat resistances higher than 1500 °C and melting points higher than 2500°C).

The developed monitoring system can be used for effective vertical positioning of the wire tool or the evaluation of wire tool amplitude during processing. It was proved that vibration monitoring allows controlling the moment of wire approach and its breakage.

The EDM experiments of conductive ceramics with brass wire tool showed repeated contacts between electrodes and helped to unveil the steps of material sublimation. CNC systems based on the detection of electrical pulses could not sense fast enough the electro-physical behaviour in the discharge gap due to the distinctive property of ceramics: high electrical resistance with a small value of required discharge

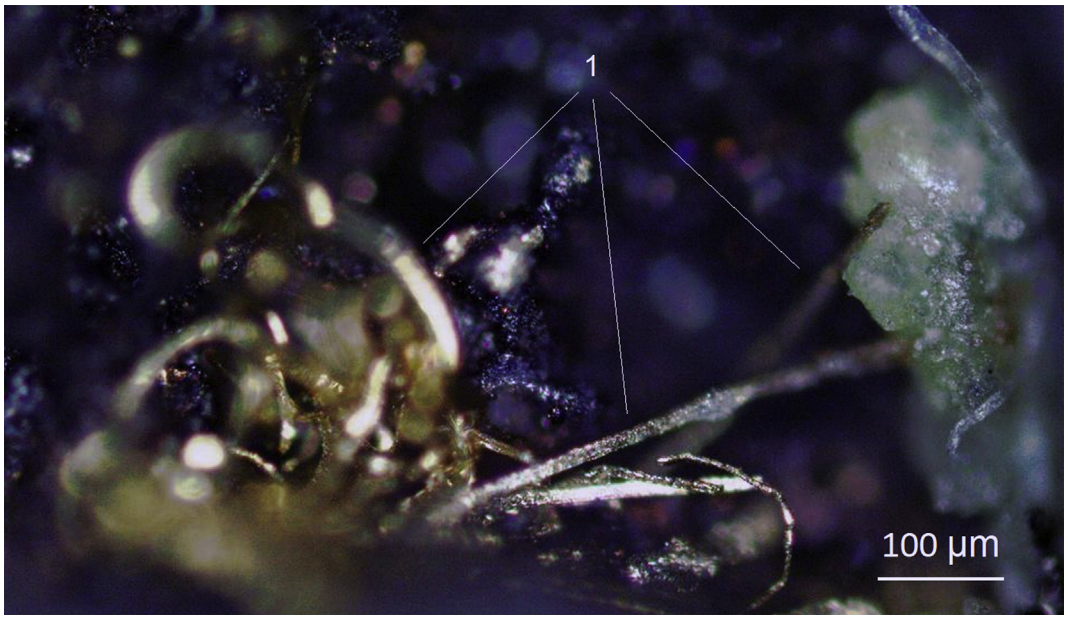

Fig. 17. Optical microscopy of metal fibers of easy-to-melt components formed in the machined groove of VOK-6O conductive ceramic composite after WEDM: (1) is fibers of 6–10 μm in plane.

2590 °C, and thus, the boiling point of brass is 2590 °C [223]. Because the melting point of brass is 850–950 °C [224, 225] and the boiling point is 2590 °C, the most rational option would be the use of a 0.25 mm diameter commercially available tungsten wire. The melting point of tungsten is 3410 °C and its boiling point is 5660 °C; the electrical resistance is 4.9×10^{-8} Ω m for 20 °C [226, 227].

5. Conclusions

The presented research showed the functional opportunities of monitoring based on acoustic emission in searching for the optimal EDM factors for new classes of conductive ceramic nanocomposites. The developed method can provide a better quality of machined surface and geometric tolerance of product and prosper for the broad application of monitoring and control methods in real production. The use of the developed monitoring method appears reasonable for the improvement gap. The prolonged physical contact between under-voltage electrodes results in frequent wire breakage and multiple cracks at the machined surfaces of a workpiece.

The control of the contact loss at the reversal motion is necessary as well. The loss of contact after short circuiting could be accompanied by the formation of tiny fibres of the easy-to-melt material components. That phenomenon extends the period of physical interaction between electrodes and can trigger subsequent repeated short circuits.

The developed method can supplement or even replace the existing monitoring methods of electrical parameters and contribute to the creation of a multi-factor adaptive control system. It can lead to the formation of a new vision and approach in the development of a new generation of CNC systems [74, 83, 228, 229].

The validation of the developed system on the samples of conductive ceramics and analytical investigation on the nature of electrical erosion promote better understanding on the phenomena of material sublimation

under discharge impulses.

Declarations

Author contribution statement

Anna A Okunkova: Performed the experiments; Wrote the paper.

Sergey N. Grigoriev: Conceived and designed the experiments; Analyzed and interpreted the data.

Mikhail P. Kozochkin: Conceived and designed the experiments; Wrote the paper.

Artur N. Porvatov: Performed the experiments; Contributed reagents, materials, analysis tools or data.

Marina Volosova: Analyzed and interpreted the data; Contributed reagents, materials, analysis tools or data.

Funding statement

This work was supported by the Russian Science Foundation (project No. 18-19-00599).

Competing interest statement

The authors declare no conflict of interest.

Additional information

No additional information is available for this paper.

References

[1] S.N. Grigoriev, D.A. Masterenko, V.I. Teleshevskii, et al., Contemporary state and outlook for development of metrological assurance in the machine-building industry, Meas. Tech. 55 (2013) 1311.
[2] T. Chaudhary, A.N. Siddiquee, A.K. Chanda, Effect of wire tension on different output responses during wire electric discharge machining on AISI 304 stainless steel, Defence Technology 15 (2019) 541.
[3] U. Maradia, E. Filisetti, M. Boccadoro, M. Roten, J.-M. Dutoit, S. Hengsberger, Increasing the injection moulding productivity through EDM surface modulation, Proc. CIRP 68 (2018) 58.
[4] E. Uhlmann, D. Oberschmidt, R. Bolz, Application of micro structured, boron doped CVD-diamond as mu EDM tool electrodes, Proc. CIRP 68 (2018) 649.
[5] A.K. Sahu, S. Chatterjee, P.K. Nayak, S.S. Mahapatra, Study on effect of tool electrodes on surface finish during electrical discharge machining of Nitinol, IOP Conf. Ser. Mater. Sci. Eng. 338 (2018), 012033.
[6] R.P. Prathipati, V. Devuri, M. Cheepu, K. Gudimetla, R.U. Kiran, Machining of AISI D2 tool steel with multiple hole electrodes by EDM process, IOP Conf. Ser. Mater. Sci. Eng. 330 (2018), 012067.
[7] K.H. Trung, Development of a WEDM system with high machining efficiency, Int. Conf. Syst. Sci. Eng. 397 (2017).
[8] H. Wu, T. Wang, J. Wang, Research on discharge state detection of finishing in high-speed wire electrical discharge machine, Int. J. Adv. Manuf. Technol. 103 (2019) 2301.
[9] A. Takale, N. Chougule, Optimization of process parameters of wire electro discharge machining for Ti49.4Ni50.6 shape memory alloys using the Taguchi technique, Int. J. Struct. Integ. 10 (2019) 548.
[10] M.A. Volosova, A.A. Okunkova, D.E. Povolotskiy, P.A. Podrabinnik, Study of electrical discharge machining for the parts of nuclear industry usage, Mech. Ind. 16 (2015) 706.
[11] V.N. Gavrin, Yu.P. Kozlova, E.P. Veretenkin, et al., Reactor target from metal chromium for "pure" high-intensive artificial neutrino source, Phys. Part. Nucl. Lett. 13 (2016) 267.
[12] H.B. Ozerkan, Simultaneous machining and surface alloying of AISI 1040 steel by electrical discharge machining with boron oxide powders, J. Mech. Sci. Technol. 32 (2018) 4357.
[13] S. Bhattacharya, G.J. Abraham, A. Mishra, et al., Corrosion behavior of wire electrical discharge machined surfaces of P91 steel, J. Mater. Eng. Perform. 27 (2018) 4561.
[14] H.-P. Nguyen, V.-D. Pham, N.-V. Ngo, Application of TOPSIS to Taguchi method for multi-characteristic optimization of electrical discharge machining with titanium powder mixed into dielectric fluid, Int. J. Adv. Manuf. Technol. 98 (2018) 1179.
[15] G. Zhang, Y. Zhang, Z. Chen, et al., Magnetic-assisted method and multi-objective optimization for improving the machining characteristics of WEDM in trim cutting magnetic material, Int. J. Adv. Manuf. Technol. 98 (2018) 1471.
[16] M. Sarikaya, V. Yilmaz, Optimization and predictive modeling using S/N, RSM, RA and ANNs for micro-electrical discharge drilling of AISI 304 stainless steel, Neural Comput. Appl. 30 (2018) 1503.
[17] H. Ma, X. Zhou, W. Liu, et al., A feature-based approach towards integration and automation of CAD/CAPP/CAM for EDM electrodes, Int. J. Adv. Manuf. Technol. 98 (2018) 2943.
[18] X. Chen, Z. Wang, J. Xu, et al., Sustainable production of micro gears combining micro reciprocated wire electrical discharge machining and precision forging, J. Clean. Prod. 188 (2018) 1.
[19] M. Gostimirovic, P. Kovac, M. Sekulic, An inverse optimal control problem in the electrical discharge machining, Sadhana Acad. Proc. Eng. Sci. 43 (2018). UNSP 70.
[20] G. Selvakumar, K.G.T. Kuttalingam, S.R. Prakash, Investigation on machining and surface characteristics of AA5083 for cryogenic applications by adopting trim cut in WEDM, J. Braz. Soc. Mech. Sci. Eng. 40 (2018). UNSP 267.
[21] K. Oshima, M. Kunieda, Attempts to fabricate micro injection molding tools and assemble molded micro parts on same EDM machine, CIRP Ann. Manuf. Technol. 67 (2018) 213.
[22] R. Swiercz, D. Oniszczuk-Swiercz, Experimental Investigation of surface layer properties of high thermal conductivity tool steel after electrical discharge machining, Metals 7 (2017) 550.
[23] M. Song, H. Zhao, J. Liu, et al., Replication of large scale micro pillar array with different diameters by micro injection molding, Microsyst. Tech. Micro. Nanosyst. Inf. Storage Process. Syst. 23 (2017) 2087.
[24] J.-C. Lee, S.-H. Park, J.K. Min, et al., Development of a perpendicular vibration-induced electrical discharge machining process for fabrication of partially wavy inner structures, J. Mech. Sci. Technol. 30 (2016) 2257.
[25] V.N. Gavrin, Yu.P. Kozlova, E.P. Veretenkin, et al., Reactor target from metal chromium for "pure" high-intensive artificial neutrino source, Phys. Part. Nucl. 48 (2017) 5.
[26] M. Lundberg, J. Saarimaki, J.J. Moverare, et al., Surface integrity and fatigue behaviour of electric discharged machined and milled austenitic stainless steel, Mater. Char. 124 (2017) 215.
[27] J.F. Liu, Y.B. Guo, Thermal modeling of EDM with progression of massive random electrical discharges, Proc. Manuf. 5 (2016) 495.
[28] A.N. Porvatov, M.P. Kozochkin, S.V. Fedorov, A.A. Okunkova, About possibility of vibroacoustic diagnostics of electrical discharge machining and characterization of defects, Mech. Ind. 16 (2015) 707.
[29] S.N. Grigoriev, M.P. Kozochkin, E. Yu. Kropotkina, A.A. Okunkova, Study of wire tool-electrode behavior during electrical discharge machining by vibroacoustic monitoring, Mech. Ind. 17 (2016) 717.
[30] S. Plaza, N. Ortega, J.A. Sanchez, et al., Original models for the prediction of angular error in wire-EDM taper-cutting, Int. J. Adv. Manuf. Technol. 44 (2009) 529.
[31] D.A.H. Hanaor, E.A. Flores Johnson, S. Wang, et al., Mechanical properties in crumple-formed paper derived materials subjected to compression, Heliyon 3 (6) (2017) e00329.
[32] A.M. Matz, D. Kammerer, N. Jost, et al., Machining of metal foams with varying mesostructure using wire EDM, Proc. CIRP 42 (2016) 263.
[33] F. Tavangarian, A. Fahami, G. Li, et al., Structural characterization and strengthening mechanism of forsterite nanostructured scaffolds synthesized by multistep sintering method, J. Mater. Sci. Technol. 34 (2018) 2263.
[34] P. Hu, W. Sun, M. Fan, et al., Large energy density at high-temperature and excellent thermal stability in polyimide nanocomposite contained with small loading of BaTiO3 nanofibers, Appl. Surf. Sci. 458 (2018) 743.
[35] S. Mathiazhagan, S. Anup, Atomistic Simulations of Length-Scale Effect of Bioinspired Brittle-Matrix Nanocomposite Models, J. Eng. Mech. 144 (2018), 04018104.
[36] N. Wu, X. Li, J.-G. Li, et al., Fabrication of Gd2O3-MgO nanocomposite optical ceramics with varied crystallographic modifications of Gd2O3 constituent, J. Am. Ceram. Soc. 101 (2018) 4887.
[37] Y.-X. Li, Y. Cao, M. Wang, et al., Novel high-flux polyamide/TiO2 composite nanofiltration membranes on ceramic hollow fibre substrates, J. Membr. Sci. 565 (2018) 322.
[38] W.-D. Oh, J. Lei, A. Veksha, et al., Ni-Zn-based nanocomposite loaded on cordierite mullite ceramic for syngas desulfurization: Performance evaluation and regeneration studies, Chem. Eng. J. 351 (2018) 230.
[39] J. Luo, S. Luo, C. Zhang, et al., Analysis of the intragranular microstructure in ceramic nanocomposites and their effect on the mechanical properties, J. Am. Ceram. Soc. 101 (2018) 5151.
[40] A. Goral, S.J. Skrzypek, The influence of alumina nanoparticles on lattice defects, crystallographic texture and residual stresses in electrodeposited Ni/Al2O3 composite coatings, Appl. Surf. Sci. 456 (2018) 147.
[41] Y.C. Cheng, C.P. Jiang, D.H. Lin, Finite element based optimization design for a one-piece zirconia ceramic dental implant under dynamic loading and fatigue life validation, Struct. Multidiscip. Optim. 59 (3) (2019) 835.
[42] E. Marin, S. Horiguchi, M. Zanocco, et al., Bioglass functionalization of laser-patterned bioceramic surfaces and their enhanced bioactivity, Heliyon 4 (12) (2018) e01016.
[43] D. Ragurajan, M. Golieskardi, M. Satgunam, et al., Advanced 3Y-TZP bioceramic doped with Al2O3 and MnO2 particles potentially for biomedical applications: study on mechanical and degradation properties, J. Mater. Res. Technol. JMR&T 7 (4) (2018) 432.
[44] R. Ivanov, I. Hussainova, M. Aghayan, et al., Graphene-encapsulated aluminium oxide nanofibers as a novel type of nanofillers for electroconductive ceramics, J. Eur. Ceram. Soc. 35 (14) (2015) 4017.

[45] C. Zhang, Effect of wire electrical discharge machining (WEDM) parameters on surface integrity of nanocomposite ceramics, Ceram. Int. 40 (7) (2014) 9657.
[46] D. Hanaoka, Y. Fukuzawa, C. Ramirez, et al., Electrical discharge machining of ceramic/carbon nanostructure composites, Proc. CIRP 6 (2013) 95.
[47] B.A. Movchan, N.I. Grechanyuk, Microhardness and microbrittleness of condensates of the TiC-Al2O3 system, Inorg. Mater. 17 (7) (1981) 972.
[48] M. Watanabe, I. Fukuura, Strength of Al2O3 and Al2O3-tic ceramics in relation to their fracture sources, Am. Ceram. Soc. Bull. 60 (3) (1981) 394.
[49] Technical standard GOST 25003-81 of the Euro-Asian Council for Standardization, Metrology and Certification (EASC). The Plates Cutting Replaceable many-sided Ceramic. Technical conditions (RU).
[50] M. Lee, M. Borom, Rapid rate sintering of Al2O3–TiC composites for cutting-tool application, Adv. Ceram. Mater. 3 (1988) 38.
[51] R.A. Cutler, A.C. Hurford, A.V. Virkar, Pressureless-sintered Al2O3-TiC composites, Mater. Sci. Eng. A 105–106 (1) (1988) 183.
[52] B.I. Smirnov, V.I. Nikolaev, Y.A. Burenkov, et al., Some physical properties of an Al2O3-SiC-TiC composite, Tech. Phys. Lett. 23 (12) (1997) 923.
[53] K.F. Cai, D.S. McLachlan, N. Axen, et al., Preparation, microstructures and properties of Al2O3-TiC composites, Ceram. Int. 28 (2) (2002) 217.
[54] Y.F. Zhang, L.J. Wang, W. Jiang, et al., Effect of fabrication method on microstructure and properties of Al2O3-TiC composites, Mater. Trans. 46 (9) (2005) 2015.
[55] Y.F. Zhang, L.J. Wang, W. Jiang, et al., Microstructure and properties of Al2O3-TiC composites fabricated by combination of high-energy ball milling and spark plasma sintering (SPS), J. Inorg. Mater. 20 (6) (2005) 1445.
[56] Y.F. Zhang, L.J. Wang, W. Jiang, et al., Microstructure and properties of Al2O3-TiC nanocomposites fabricated by spark plasma sintering from high-energy ball milled reactants, J. Eur. Ceram. Soc. 26 (15) (2006) 3393.
[57] V. Yu. Fominski, S.N. Grigoriev, J.P. Celis, et al., Structure and mechanical properties of W-Se-C/diamond-like carbon and W-Se/diamond-like carbon bi-layer coatings prepared by pulsed laser deposition, Thin Solid Films 520 (21) (2012) 6476.
[58] D. Kotoban, S. Grigoriev, A. Okunkova, et al., Influence of a shape of single track on deposition efficiency of 316L stainless steel powder in cold spray, Surf. Coat. Technol. 309 (2017) 951.
[59] A.S. Metel, M.M. Stebulyanin, S.V. Fedorov, et al., Power density distribution for laser additive manufacturing (SLM): potential, fundamentals and advanced applications, Technologies 7 (1) (2018) 5.
[60] Y.K. Lok, T.C. Lee, Processing of advanced ceramics using the Wire-Cut EDM process, J. Mater. Process. Technol. 63 (1–3) (1997) 839.
[61] J.D. Yun, C. Go, D.H. Wang, et al., Electrical discharge machining of aluminum oxide matrix composites containing titanium carbide as a conductive second phase, Proc. Fabr. Adv. Mater. VI (1–2) (1998) 1773.
[62] T. Lee, J.X. Deng, Mechanical surface treatments of electro-discharge machined (EDMed) ceramic composite for improved strength and reliability, J. Eur. Ceram. Soc. 22 (4) (2002) 545.
[63] K.M. Patel, P.M. Pandey, P.V. Rao, Study on machinabilty of Al2O3 ceramic composite in EDM using response surface methodology, J. Eng. Mater. Technol. Trans. ASME 133 (2) (2011), 021004.
[64] K.M. Patel, P.M. Pandey, P.V. Rao, Optimisation of process parameters for multi-performance characteristics in EDM of Al2O3 ceramic composite, Int. J. Adv. Manuf. Technol. 47 (9–12) (2010) 1137.
[65] K.M. Patel, P.M. Pandey, P.V. Rao, Surface integrity and material removal mechanisms associated with the EDM of Al2O3 ceramic composite, Int. J. Refract. Metals Hard Mater. 27 (5) (2009) 892.
[66] V.V. Kuzin, S.N. Grigor'ev, M.A. Volosova, Effect of a TiC coating on the stress-strain state of A plate of a high-density nitride ceramic under nonsteady thermoelastic conditions, Refract. Ind. Ceram. 54 (5) (2014) 376.
[67] S.V. Fedorov, M.D. Pavlov, A.A. Okunkova, Effect of structural and phase transformations in alloyed subsurface layer of hard-alloy tools on their wear resistance during cutting of high-temperature alloys, J. Frict. Wear 34 (3) (2013) 190.
[68] V. Yu. Fominski, S.N. Grigoriev, A.G. Gnedovets, et al., Pulsed laser deposition of composite Mo-Se-Ni-C coatings using standard and shadow mask configuration, Surf. Coat. Technol. 206 (24) (2012) 5046.
[69] S.N. Grigoriev, V.D. Gurin, M.A. Volosova, et al., Development of residual cutting tool life prediction algorithm by processing on CNC machine tool, Materialwissenchaft Und Werkstofftechnik 44 (9) (2013) 790.
[70] L.A. Mendes, F.L. Amorim, W.L. Weingaertner, Automated system for the measurement of spark current and electric voltage in wire EDM performance, J. Braz. Soc. Mech. Sci. Eng. 37 (2015) 123.
[71] K.-H. Tseng, C.-Y. Chang, M.-J. Chen, et al., Novel electrical discharge machining system with real-time control and monitoring for preparing nanoiron colloid, Adv. Mech. Eng. 10 (2018), 1687814018791705.
[72] S.N. Grigoriev, V.A. Sinopalnikov, M.V. Tereshin, et al., Control of parameters of the cutting process on the basis of diagnostics of the machine tool and workpiece, Meas. Tech. 55 (5) (2012) 555.
[73] M.P. Kozochkin, A.N. Porvatov, F.S. Sabirov, The fitting of technological equipment with data-measuring systems, Meas. Tech. 55 (5) (2012) 530.
[74] Yu.A. Melnik, M.P. Kozochkin, A.N. Porvatov, et al., On adaptive control for electrical discharge machining using vibroacoustic emission, Technologies 6 (4) (2018) 96.
[75] M.P. Kozochkin, S.N. Grigor'ev, A.A. Okun'kova, Russian aeronautics, Iz VUZ 58 (2015) 488.
[76] A. Isaev, V. Grechishnikov, P. Pivkin, et al., Machining of thin-walled parts produced by additive manufacturing technologies, Proc. CIRP 41 (2016) 1023.
[77] A. Sova, M. Doubenskaia, S. Grigoriev, et al., Parameters of the gas-powder supersonic jet in cold spraying using a mask, J. Therm. Spray Technol. 22 (4) (2013) 551.
[78] A.V. Gusarov, S.N. Grigoriev, M.A. Volosova, et al., On productivity of laser additive manufacturing, J. Mater. Process. Technol. 261 (2018) 213.
[79] V.N. Kostyukov, A.P. Naumenko, I.S. Kudryavtseva, Assessment of characteristic function modulus of vibroacoustic signal given a limit state parameter of diagnosed equipment, J. Phys. Conf. Ser. 944 (2018). UNSP 012063.
[80] P. Wolszczak, G. Litak, M. Dziuba, Monitoring of drilling conditions using the Hilbert-Huang transformation, MATEC Web Conf 148 (2018). UNSP 16003.
[81] M.P. Kozochkin, A.N. Porvatov, F.S. Sabirov, Vibration testing of technological processes in automated machining equipment, Meas. Tech. 56 (2014) 1414.
[82] A. Pramanik, A.K. Basak, Sustainability in wire electrical discharge machining of titanium alloy: Understanding wire rupture, J. Clean. Prod. 198 (2018) 472.
[83] M.P. Kozochkin, A.N. Porvatov, Estimation of uncertainty in solving multi-parameter diagnostic problem, Meas. Tech. 58 (2015) 173.
[84] T. Muthuramalingam, A. Ramamurthy, K. Sridharan, et al., Analysis of surface performance measures on WEDM processed titanium alloy with coated electrodes, Mater. Res. Express 5 (2018) 126503.
[85] A.I. Surenkov, V.V. Ignat'ev, S.S. Abalin, et al., Corrosion resistance and mechanical stability of nickel alloys in molten-salt nuclear reactors, Atom. Energy 124 (2018) 43.
[86] V.B. Tarel'nik, A.V. Paustovskii, Yu.G. Tkachenko, et al., Electrospark graphite alloying of steel surfaces: technology, properties, and application, Surf. Eng. Appl. Electrochem. 54 (2018) 147.
[87] A.A. Kovalev, N.N. Kuznetsov, Cavitation Fracture of the Typical Materials Used in Hydraulic Machines and Units, Russ. Metall. 13 (2017) 1202.
[88] P. Huilgol, K.R. Udupa, K.U. Bhat, Metastable microstructures at the interface between AISI 321 steel and molten aluminum during hot-dip aluminizing, Surf. Coat. Technol. 348 (2018) 22.
[89] A.A. Tiamiyu, V.S. Tari, J.A. Szpunar, et al., Effects of grain refinement on the quasi-static compressive behavior of AISI 321 austenitic stainless steel: EBSD, TEM, and XRD studies, Int. J. Plast. 107 (2018) 79.
[90] M.S. Ghazani, B. Eghbali, Characterization of the hot deformation microstructure of AISI 321 austenitic stainless steel, Mater. Sci. Eng. A Struct. Mater. Prop. Microstruct. Proc. 730 (2018) 380.
[91] W. Zhang, S. Jiang, X. Li, et al., An approach to structural reliability evaluation under fatigue degradation and shocks, Mech. Syst. Signal Process. 113 (2018) 65.
[92] O.V. Dement'eva, A.M. Semiletov, A.A. Chirkunov, et al., Structure and Electrical Conductivity of Ring Deposits Resulting from Evaporation of Droplets of Dispersions Containing Gold Nanoparticles with Different Degrees of Anisotropy, Colloid J 80 (2018) 474.
[93] E. Zasimchuk, O. Baskova, O. Gatsenko, et al., Universal Mechanism of Viscoplastic Deformation of Metallic Materials Far from Thermodynamics Equilibrium, J. Mater. Eng. Perform. 27 (2018) 4183.
[94] A.S. Metel, S.N. Grigoriev, Yu.A. Melnik, et al., Broad beam sources of fast molecules with segmented cold cathodes and emissive grids, Instrum. Exp. Tech. 55 (1) (2012) 122.
[95] H. Nam, S.J. Kwon, E.S. Cho, Direct Ablation of Aluminum-Doped Zinc Oxide Thin Films for Electrode Patterning by Optimization of Laser Beam Conditions, J. Nanosci. Nanotechnol. 17 (2017) 8432.
[96] Z.N. Bai, Z.X. Bai, Z.J. Kang, et al., Non-Pulse-Leakage 100-kHz Level, High Beam Quality Industrial Grade Nd:YVO4 Picosecond Amplifier, Appl. Sci. Basel 7 (2017) 615.
[97] I.A. Pinahin, V.A. Chernigovskij, A.A. Bracihin, et al., Improvement of wear resistance of VK6, VK8, T5K10, and T15K6 hard alloys by volume pulsed laser hardening, J. Frict. Wear 36 (2015) 330.
[98] I.V. Blinkov, D.S. Belov, A.O. Volkhonskii, et al., Structure of Nanocrystalline Arc-PVD (Ti, Al)N Coatings Modified with Nickel, Russ. Metall. 5 (2015) 421.
[99] A.N. Ishchenko, S.A. Afanas'eva, N.N. Belov, et al., Intrusion features of a high-speed striker of a porous tungsten-based alloy with a strengthening filler in a steel barrier, Tech. Phys. Lett. 43 (2017) 796.
[100] U. Caydas, Machinability evaluation in hard turning of AISI 4340 steel with different cutting tools using statistical techniques, Proc. Inst. Mech. Eng. B J. Eng. Manuf. 224 (2010) 1043.
[101] A.G. Sokolov, E.E. Bobylyov, The element-phase composition and properties of the surface layers of carbide-tipped tools made of TK and WC-Co alloys, Lett. Mater. Pis Ma O Materialakh 7 (2017) 222.
[102] E.V. Ageev, R.A. Latypov, A.S. Ugrimov, Metallurgical features of the manufacture of hard-alloy powders by electroerosive dispersion of a T15K6 alloy in butanol, Russ. Metall. 12 (2016) 1155.
[103] A.M. Sergeeva, N.S. Lovizin, A.A. Sosnin, Combined technology of aluminum alloy vertical casting and simultaneous deformation, Metallurgist 62 (2018) 270.
[104] F.V. Grechnikov, E.A. Nosova, Effect of composition and distribution of phases after aging on stamp ability for aluminum alloy D16 (AA2014) sheets, Russ. J. Non-Ferrous Metals 58 (2017) 625.
[105] C. Li, Z. Liu, L. Fang, et al., Super-high-thickness high-speed wire electrical discharge machining, Int. J. Adv. Manuf. Technol. 95 (2018) 1805.
[106] S.M. Chernega, I.A. Poliakov, M.A. Krasovskiy, Increasing the wear resistance of the T15K6 hard alloy by boriding and complex saturation with boron and copper, J. Superhard Mater. 38 (2016) 190.
[107] Yu.G. Tkachenko, D.Z. Yurchenko, V.F. Britun, et al., Electrospark-deposited coatings from titanium and tungsten carbide alloys: mass transfer kinetics, structurization, and properties, Powder Metall. Met. Ceram. 54 (2015) 309.
[108] H.-T. Nguyen, Q.-C. Hsu, Study on cutting forces and material removal rate in hard milling of SKD 61 alloy steel, J. Chin. Soc. Mech. Eng. 38 (2017) 41.

[109] C.-S. Chang, C.-K. Chung, J.-F. Lin, Jen-Fin, Surface quality, microstructure, mechanical properties and tribological results of the SKD 61 tool steel with prior heat treatment affected by the deposited energy of continuous wave laser micro-polishing, J. Mater. Process. Technol. 234 (2016) 177.

[110] Y.-C. Lin, J.-C. Hung, H.-M. Lee, et al., Machining characteristics of a hybrid process of EDM in gas combined with ultrasonic vibration, Int. J. Adv. Manuf. Technol. 92 (2017) 2801.

[111] S.-T. Chen, C.-Y. Chu, Fabrication and testing of a novel biopotential electrode array, J. Mater. Process. Technol. 250 (2017) 345.

[112] Z.-Z. Wu, X.-Y. Wu, J.-G. Lei, et al., Vibration-assisted micro-ECM combined with polishing to machine 3D microcavities by using an electrolyte with suspended B4C particles, J. Mater. Process. Technol. 255 (2018) 275.

[113] J.I. Ahuir-Torres, M.A. Arenas, W. Perrie, et al., Influence of laser parameters in surface texturing of Ti6A14V and AA2024-T3 alloys, Opt. Lasers Eng. 103 (2018) 100.

[114] B. Wu, P. Liu, F. Zhang, et al., Effect of parameters on picosecond laser ablation of Cr12MoV cold work mold steel, Appl. Phys. Mater. Sci. Proc. 124 (2018) 11.

[115] C. Sima, O. Toma, Influence of temperature on the CuIn(1-x)Ga(x)Se(2)films deposited by picosecond laser ablation, Appl. Surf. Sci. 425 (2017) 1028.

[116] M.A. Volosova, S.N. Grigor'ev, V.V. Kuzin, Effect of titanium nitride coating on stress structural inhomogeneity in oxide-carbide ceramic. Part 4. Action of heat flow, Refract. Ind. Ceram. 56 (1) (2015) 91.

[117] M.A. Volosova, V.D. Gurin, Influence of vacuum-plasma nitride coatings on contact processes and a mechanism of wear of working surfaces of high-speed steel cutting tool at interrupted cutting, J. Frict. Wear 34 (3) (2013) 183.

[118] B. Zhao, H. Liu, C. Huang, et al., Evolution mechanisms of high temperature mechanical properties and microstructures of Al2O3/SiCw/TiCn nanocomposite materials, J. Alloy. Comp. 737 (2018) 46.

[119] B. Zhao, H. Liu, C. Huang, et al., Fabrication and mechanical properties of Al2O3-SiCw-TiCnp ceramic tool material, Ceram. Int. 43 (2017) 10224.

[120] A.I. Pronin, V.V. Myl'nikov, E.B. Shchelkunov, et al., Investigation of Cutting Ceramic Stability During Sharpening of Hardened Steel Blanks, Glass Ceram. 74 (2018) 364.

[121] V.N. Gadalov, D.N. Romanenko, V.V. Samoilov, et al., Procedure of evaluating the surface roughness of the electrospark coating after burnishing with mineral ceramics, Russ. J. Non-Ferrous Metals 53 (2012) 348.

[122] V. Dutta, S. Sharma, K. Chopra, et al., Hybrid Electric Discharge Machining Processes for Hard Materials: A Review, Mat. Focus 5 (2016) 202.

[123] S.N. Grigoriev, V. Yu. Fominski, R.I. Romanov, et al., Shadow masked pulsed laser deposition of WSex films: experiment and modeling, Appl. Surf. Sci. 282 (2013) 607.

[124] A.S. Metel, S.N. Grigoriev, Yu.A. Melnik, Glow discharge with electrostatic confinement of electrons in a chamber bombarded by fast electrons, Plasma Phys. Rep. 37 (7) (2011) 628.

[125] M.D. Nguyen, M. Rahman, Y.S. Wong, Transitions of micro-EDM/SEDCM/micro-ECM milling in low-resistivity deionized water, Int. J. Mach. Tool Manuf. 69 (2013) 48.

[126] S. El-Khatib, A.Y. Shash, A.H. Elsayed, et al., Effect of carbon nano-tubes and dispersions of SiC and Al2O3 on the mechanical and physical properties of copper-nickel alloy, Heliyon 4 (10) (2018) e00876.

[127] L. Selvarajan, C.S. Narayanan, R. Jeyapaul, et al., Optimization of EDM process parameters in machining Si3N4-TiN conductive ceramic composites to improve form and orientation tolerances, Measurement 92 (2016) 114.

[128] A. Metel, S. Grigoriev, Yu. Melnik, et al., Cutting tools nitriding in plasma produced by a fast neutral molecule beam, Jpn. J. Appl. Phys. 50 (8) (2011), 08JG04.

[129] A.B. Pandey, P.K. Brahmankar, A method to predict possibility of arcing in EDM of TiB(2)p reinforced ferrous matrix composite, Int. J. Adv. Manuf. Technol. 86 (2016) 2837.

[130] R.M. Gunnagol, B. Sharma, M.K. Rabinal, Flexible contact stamp for electrical conductivity measurements of a soft matter, Measurement 92 (2016) 224.

[131] R. Endo, M. Shima, M. Susa, Thermal-conductivity measurements and predictions for Ni-Cr solid solution alloys, Int. J. Thermophys. 31 (2010) 1991.

[132] N. Deprez, D.S. Mclachlan, The analysis of the electrical-conductivity of graphite powders during compaction, J. Phys. D Appl. Phys. 21 (1988) 101.

[133] S.N. Grigor'ev, M.P. Kozochkin, S.V. Fedorov, et al., Study of electroerosion processing by vibroacoustic diagnostic methods, Meas. Tech. 58 (2015) 878.

[134] S.N. Grigor'ev, M.P. Kozochkin, Improvement of machining by the vibroacoustic diagnostics of electrophysical processes, Russ. Eng. Res. 35 (2015) 801.

[135] M.P. Kozochkin, A.N. Porvatov, Effect of adhesion bonds in friction contact on vibroacoustic signal and autooscillations, J. Frict. Wear 35 (2014) 389.

[136] N.M. Abbas, M. Kunieda, Increasing discharge energy of micro-EDM with electrostatic induction feeding method through resonance in circuit, Precis. Eng. 45 (2016) 118.

[137] J. Che, T. Zhou, X. Zhu, et al., Experimental study on horizontal ultrasonic electrical discharge machining, J. Mater. Process. Technol. 231 (2016) 312.

[138] Y.-S. Fan, J.-C. Bai, Study on volt-ampere characteristics of spark discharge for transistor resistor pulse power of EDM, Int. J. Adv. Manuf. Technol. 96 (2018) 3019.

[139] M.P. Kozochkin, Nonlinear dynamics of cutting, Russ. Eng. Res. 32 (2012) 387.

[140] A. Germashev, V. Logominov, D. Anpilogov, et al., Optimal cutting condition determination for milling thin-walled details, Advances In Manufacturing 6 (2018) 280.

[141] Y. Zhang, Z. Zhang, H. Huang, et al., Study on thermal deformation behavior and microstructural characteristics of wire electrical discharge machining thin-walled components, J. Manuf. Process. 31 (2018) 9.

[142] V.V. Zolotarev, V.P. Smolentsev, Vestnik Voronezhskogo Gosudarstvennogo universiteta, Bull. Voronezh State Techn. Univ.] 13 (2017) 110 (In Russian).

[143] R. Mishra, D. Kumar, D. Saurav, et al., Effects of tool electrode on EDM performance of Ti-6Al-4V, Silicon 10 (2018) 2263.

[144] Y. Sun, Y. Gong, Experimental study on fabricating spirals microelectrode and micro-cutting tools by low speed wire electrical discharge turning, J. Mater. Process. Technol. 258 (2018) 271.

[145] L. Straka, S. Hasova, Optimization of material removal rate and tool wear rate of Cu electrode in die-sinking EDM of tool steel, Int. J. Adv. Manuf. Technol. 97 (2018) 2647.

[146] M.Y. Tsai, C.S. Fang, M.H. Yen, Vibration-assisted electrical discharge machining of grooves in a titanium alloy (Ti-6A-4V), Int. J. Adv. Manuf. Technol. 97 (2018) 297.

[147] S. Tatzko, M. Jahn, On the use of complex numbers in equations of nonlinear structural dynamics, Mech. Syst. Signal Process. 126 (2019) 626.

[148] V.V. Smirnov, L.I. Manevitch, Large-amplitude nonlinear normal modes of the discrete sine lattices, Phys. Rev. 95 (2) (2017), 022212.

[149] M.I. Ivanov, Natural harmonic oscillations of a heavy fluid in basins of complex shape, Fluid Dyn. 41 (1) (2006) 121.

[150] P. Margerit, A. Lebee, J.-F. Caron, et al., High Resolution Wavenumber Analysis (HRWA) for the mechanical characterisation of viscoelastic beams, J. Sound Vib. 433 (2018) 198.

[151] G.P.M. Fierro, M. Meo, Nonlinear elastic imaging of barely visible impact damage in composite structures using a constructive nonlinear array sweep technique, Ultrasonics 90 (2018) 125.

[152] Y. Altintas, Manufacturing Automation: Metal Cutting Mechanics, Machine Tool Vibrations, and CNC Design, Cambridge University Press, Cambridge. UK, 2000.

[153] J. Webster, W.P. Dong, R. Lindsay, Raw acoustic emission signal analysis of grinding process, CIRP Ann. Manuf. Technol. 45 (1996) 335.

[154] V.A. Belyi, O.V. Kholodilov, A.I. Sviridyonok, Acoustic Spectrometry as Used for the Evaluation of Tribological Systems, Wear 69 (1981) 309.

[155] H.V. Ravindra, Y.G. Srinivasa, R. Krishnamurthy, Acoustic emission for tool condition monitoring in metal cutting, Wear 212 (1997) 78.

[156] F. Fan, K.Y. See, J.K. Banda, et al., Simulation of three-phase motor drive system with bearing discharge process, in: Progress in Electromagnetics Research Symposium, 2017, p. 2091.

[157] C. Smith, P. Koshy, Applications of acoustic mapping in electrical discharge machining, CIRP Ann. Manuf. Technol. 62 (2013) 171.

[158] H. Li, Z. Li, B. Zhang, et al., Suppressing Electromagnetic Interference in Direct Current Converters, IEEE Circuits Syst. Mag. 9 (2009) 10.

[159] A. Ramachandran, M.C. Reddy, R. Moodithaya, Minimization and identification of conducted emission bearing current in variable speed induction motor drives using PWM inverter, Sadhana - Acad. Proc. Eng. Sci. 33 (2008) 615.

[160] S.K. Bhattacharyya, M.F. El-Menshawy, Monitoring the EDM Process by Radio Signals, Int. J. Prod. Res. 16 (1978) 353.

[161] M.P. Kozochkin, S.N. Grigor'ev, A.A. Okun'kova, A.N. Porvatov, Monitoring of electric discharge machining by means of acoustic emission, Russ. Eng. Res. 36 (2016) 244.

[162] M.P. Kozochkin, A.N. Porvatov, S.N. Grigor'ev, Vibroacoustic monitoring of the major parameters of electrical discharge machining, Meas. Tech. 59 (2017) 1228.

[163] M.P. Kozochkin, Study of frictional contact during grinding and development of phenomenological model, J. Frict. Wear 38 (2017) 333.

[164] A. Klepka, K. Dziedziech, L. Pieczonka, et al., Experimental investigations of contact-type damage nonlinearity, J. Phys. Conf. Ser. 842 (2017). UNSP 012054.

[165] P. Rekadze, L. Rodionov, Experimental vibroacoustic research of a gear pump made of different materials, Proc. Eng. 176 (2017) 636.

[166] K.C. Gryllias, E. Chatelet, Fr. Massi, et al., in: Proceedings of International Conference on Noise and Vibration Engineering (ISMA2014) and International Conference on Uncertainty in Structural Dynamics (USD2014), 2014, p. 1877.

[167] V.P. Sergienko, S.N. Bukharov, A.V. Kupreev, Noise and Vibration in Brake Systems of Vehicles. Part 1: Experimental Procedures, J. Frict. Wear 29 (2008) 234.

[168] L. Grabec, P. Leskovar, Acoustic-emission of a cutting process, Ultrasonic 15 (1977) 17.

[169] S. Diop, E. Rigaud, P.-H. Cornuault, et al., Experimental analysis of the vibroacoustic response of an electric window-lift gear motor generated by the contact between carbon brushes and commutator, J. Vib. Acoust. Trans. ASME 139 (6) (2017), 061002.

[170] M.S. Mahdieh, R.A. Mahdavinejad, A study of stored energy in ultra-fined grained aluminum machined by electrical discharge machining, Proc. Inst. Mech. Eng. C J. Mech. Eng. Sci. 231 (2017) 4470.

[171] I.A. Veretennikova, N.B. Pugacheva, E.O. Smirnova, et al., The laser-welded joint of an austenitic corrosion-resistant steel and a titanium alloy with an intermediate copper insert, Lett. Mater. Pis Ma O Materialakh 8 (1) (2018) 42.

[172] I.O. Bannykh, M.A. Sevost'yanov, M.E. Prutskov, Effect of heat treatment on the mechanical properties and the structure of a high-nitrogen austenitic 02Kh20AG10N4MFB steel, Russ. Metall. 7 (2016) 613.

[173] Y. Cao, S. Ni, X. Liao, M. Song, Y. Zhu, Structural evolutions of metallic materials processed by severe plastic deformation, Mater. Sci. Eng. R Rep. 133 (2018) 1.

[174] L. Pang, A. Hosseini, H.M. Hussein, I. Deiab, H.A. Kishawy, Application of a new thick zone model to the cutting mechanics during end-milling, Int. J. Mech. Sci. 96–97 (2015) 91.

[175] A. Conde, A. Arriandiaga, J.A. Sanchez, et al., High-accuracy wire electrical discharge machining using artificial neural networks and optimization techniques, Robot. Comput. Integr. Manuf. 49 (2018) 24.

[176] C. Lin, Z. Wu, Y. Ren, et al., Characteristic analysis of unidirectional multi-driven and large stroke micro/nano-transmission platform, Microsyst. Technol. Micro Nanosyst. Inf. Storage Proc. Syst. 23 (2017) 3389.
[177] W.I. Cho, V. Schultz, P. Woizeschke, Numerical study of the effect of the oscillation frequency in buttonhole welding, J. Mater. Process. Technol. 261 (2018) 202.
[178] Y. Chen, M. Yang, J. Long, et al., Analysis of oscillation frequency deviation in elastic coupling digital drive system and robust notch filter strategy, IEEE Trans. Ind. Electron. 66 (2019) 90.
[179] K.-H. Tseng, M.-Y. Chung, C.-Y. Chang, Parameters for fabricating nano-Au colloids through the electric spark discharge method with micro-electrical discharge machining, Nanomaterials 7 (2017) 133.
[180] X. Yue, X. Yang, J. Tian, et al., Thermal, mechanical and chemical material removal mechanism of carbon fiber reinforced polymers in electrical discharge machining, Int. J. Mach. Tool Manuf. 133 (2018) 4.
[181] M.P. Jahan, T. Saleh, M. Rahman, et al., Development, modeling, and experimental investigation of low frequency workpiece vibration-assisted micro-EDM of tungsten carbide, J. Manuf. Sci. Eng. Trans. ASME 132 (2010), 054503.
[182] Z. Zhang, H. Yu, Y. Zhang, et al., Analysis and optimization of process energy consumption and environmental impact in electrical discharge machining of titanium superalloys, J. Clean. Prod. 198 (2018) 833.
[183] S. Saravanan, P. Senthilkumar, M. Ravichandran, et al., Wire electrical discharge machining of AA6063-TiC particle reinforced metal matrix composites using Taguchi method, Mater. Res. Express 5 (2018) 106518.
[184] E. Abedi, S. Daneshmand, A.A.L. Neyestanak, et al., Analysis and modeling of electro discharge machining input parameters of nitinol shape memory alloy by de-ionized water and copper tools, Int. J. Electrochem. Sci. 9 (2014) 2934.
[185] B.A. Artamonov, Yu.S. Volkov, Analiz modelei elektrokhimicheskoi i elektroerozionnoi obrabotki. Chast' 2, modeli protsessov elektroerozionnoi obrabotki. Provolochnaya vyrezka (analysis of models of electrochemical and electrodischarge treatment, Part 2: models of electrodischarge treatment. Wire cutting), Moscow. RU, in: Vseross. Nauchno-Issled. Inst. Patent. Inform., 1991 (in Russian).
[186] B.G. Gutkin, Automated EDM. Mechanical Engineering, USSR, Leningrad, 1971.
[187] M. Gostimirovic, V. Pucovsky, M. Sekulic, et al., Evolutionary multi-objective optimization of energy efficiency in electrical discharge machining, J. Mech. Sci. Technol. 32 (10) (2018) 4775.
[188] M. Tanjilul, A. Ahmed, A.S. Kumar, et al., A study on EDM debris particle size and flushing mechanism for efficient debris removal in EDM-drilling of Inconel 718, J. Mater. Process. Technol. 255 (2018) 263.
[189] M. Goiogana, J.A. Sarasua, J.M. Ramos, Ultrasonic assisted electrical discharge machining for high aspect ratio blind holes, Proc. CIRP 68 (2018) 81.
[190] X. Kang, W. Liang, Y. Yang, et al., Maximum free distance method for electrode feeding path planning in EDM machining of integral shrouded blisks, Precis. Eng. J. Int. Soc. Precis. Eng. Nanotechnol. 51 (2018) 514.
[191] M.V. Korenblyum, M.L. Levit, A.L. Livshits, Adaptivnoe upravlenie elektroerozionnymi stankami (adaptive control of EDM machines), Moscow. RU, in: Nauch. Issled. Inst. Mashinostr., 1977.
[192] E.F. Nemilov, Spravochnik Po Elektroerozionnoi Obrabotke Materialov (Handbook on Electrodischarge Treatment of Materials), Mashinostroenie, Leningrad. RU, 1989.
[193] T.L. Schmitz, K.S. Smith, Machining Dynamics. Frequency Response to Improved Productivity, Springer US, New York. USA, 2009.
[194] T.M. Garcia-Ordas, E. Alegre-Gutierrez, R. Alaiz-Rodriguez, et al., Tool wear monitoring using an online, automatic and low cost system based on local texture, Mech. Syst. Signal Process. 112 (2018) 98.
[195] A. Ruf, F. Pauli, M. Schroeder, et al., Lifetime modeling of non-partial discharge-resistant insulation systems of electrical machines under dynamic load, Elektrotechnik und Informationstechnik 135 (2018) 131.
[196] T. Roy, D. Datta, R. Balasubramaniam, Numerical modelling and simulation of surface roughness of 3-D hemispherical convex micro-feature generated by reverse micro-EDM, Int. J. Adv. Manuf. Technol. 97 (2018) 979.
[197] S.S. Mujumdar, D. Curreli, S.G. Kapoor, Effect of dielectric conductivity on micro-electrical discharge machining plasma characteristics using optical emission spectroscopy, J. Micro Nano Manuf. 6 (2018). UNSP 031001.
[198] Y. Shen, J. Chen, Y. Yang, et al., Study on the characteristics of plasma channel based on multi-spark pulse discharge machining effect, Int. J. Adv. Manuf. Technol. 97 (2018) 1745.
[199] Z. Kou, F. Han, Machining characteristics and removal mechanisms of moving electric arcs in high-speed EDM milling, J. Manuf. Process. 32 (2018) 676.
[200] J. Liu, F. Deng, X. Lu, et al., A study of the material removal mechanism of polycrystalline diamond in electrical discharge machining based on spectroscopic measurement, Int. J. Adv. Manuf. Technol. 96 (2018) 697.
[201] J.F. Liang, Y.S. Liao, J.Y. Kao, et al., Study of the EDM performance to produce a stable process and surface modification, Int. J. Adv. Manuf. Technol. 95 (2018) 1743.
[202] V.M. Salmanov, A.G. Guseinov, R.M. Mamedov, et al., Effect of laser radiation on InSe and GaSe thin films grown via laser sublimation and chemical deposition, Russ. J. Phys. Chem. 92 (2018) 1790.
[203] S.N. Grigoriev, M.P. Kozochkin, A.N. Porvatov, Optimization of processing conditions on the wire electric discharge machining by the parameters of vibro-acoustic signal, Mater. Sci. Forum 876 (2016) 36.
[204] S. Delvecchio, P. Bonfiglio, F. Pompoli, Vibro-acoustic condition monitoring of Internal Combustion Engines: a critical review of existing techniques, Mech. Syst. Signal Process. 99 (2018) 661.
[205] K. Gryllias, S. Moschini, J. Antoni, Application of cyclo-nonstationary indicators for bearing monitoring under varying operating conditions, J. Eng. Gas Turbines Power Trans. ASME 140 (2018), 012501.
[206] F. Leaman, S. Hinderer, R. Baltes, et al., Acoustic emission source localization in ring gears from wind turbine planetary gearboxes, Forschung Im Ingenieurwesen Eng. Res. 83 (1) (2019) 43.
[207] Q. Hao, Y. Shen, Y. Wang, et al., A fractal model of acoustic emission signals in sliding friction, Tribol. Lett. 67 (1) (2019) 31.
[208] T. Le Gall, T. Monnier, C. Fusco, et al., Towards quantitative acoustic emission by finite element modelling: contribution of modal analysis and identification of pertinent descriptors, Appl. Sci. Basel 8 (12) (2018) 2557.
[209] V.P. Epifanov, Physical simulation of glacier motion modes, Led I Sneg Ice Snow 56 (3) (2016) 333.
[210] N.L. Kazanskiy, S.P. Murzin, Ye.L. Osetrov, et al., Synthesis of nanoporous structures in metallic materials under laser action, Opt. Lasers Eng. 49 (2011) 1264.
[211] Y. Sun, Y. Ren, New preparation method of porous copper powder through vacuum dealloying, Vacuum 122 (2015) 215.
[212] S.A. Oglezneva, M.N. Kachenyuk, N.D. Ogleznev, Investigation into the structure formation and properties of materials in the copper-titanium disilicide system, Russ. J. Non-Ferrous Metals 58 (6) (2017) 649.
[213] A.M. Shul'pekov, G.V. Lyamina, T.V. Kal'yanova, Current-conducting coatings based on heat-resistant titanium compounds obtained by self-propagating high-temperature synthesis, Russ. J. Non-Ferrous Metals 52 (3) (2011) 275.
[214] T. Fujii, K. Tohgo, M. Iwao, et al., Fracture toughness distribution of alumina-titanium functionally graded materials fabricated by spark plasma sintering, J. Alloy. Comp. 766 (2018) 1.
[215] J. Fan, D. Tang, X. Mao, et al., An Efficient Electrolytic Preparation of MAX-Phased Ti-Al-C, Metall. Mater. Trans. B Process Metall. Mater. Process. Sci. 49 (2018) 2770.
[216] E.N. Muratova, V.A. Moshnikov, V.V. Luchinin, et al., Thermal-conductive boards based on aluminum with an Al2O3 nanostructured layer for products of power electronics, Tech. Phys. 63 (11) (2018) 1626.
[217] P. Zukowski, T. Koltunowicz, J. Partyka, et al., Hopping conductivity of metal-dielectric nanocomposites produced by means of magnetron sputtering with the application of oxygen and argon ions, Vacuum 83 (2009) S280.
[218] W. Wang, N. Li, X. Li, et al., Synthesis of metallic nanotube arrays in porous anodic aluminum oxide template through electroless deposition, Mater. Res. Bull. 41 (2006) 1417.
[219] I.T. Coutinho, A.A.R. Neves, G. Sombrio, et al., Surface tension driven flow forming aluminum oxide microtubes, Int. J. Heat Mass Transf. 126 (2018) 32.
[220] S.N. Perevislov, A.S. Lysenkov, D.D. Titov, et al., Production of ceramic materials based on sic with low-melting oxide additives, Glass Ceramics 75 (2019) 400.
[221] B.S. Seplyarskii, R.A. Kochetkov, I.D. Kovalev, et al., On the nature of concentration limits of combustion wave propagation in powdered and pelletized Ti plus C plus xal(2)O(3) mixtures, Russ. J. Phys. Chem. B 12 (3) (2018) 458.
[222] G.A. Bufetova, S. Ya. Rusanov, V.F. Seregin, et al., Temperature and emissivity measurements at the sapphire single crystal fiber growth process, J. Cryst. Growth 480 (2017) 85.
[223] S. Rajamanickam, J. Prasanna, TOPSIS on High Aspect Ratio Electric Discharge Machining (EDM) of Ti-6Al-4V using 300 mu m brass rotary tube electrodes, Mater. Today Proc. 5 (9) (2018) 18489.
[224] S.K. Basha, M.V.J. Raju, M. Kolli, Experimental study of electrical discharge machining of inconel X-750 using tungsten-copper electrode, Mater. Today Proc. 5 (5) (2018) 11622.
[225] Y. Yang, C. Wang, X. Chen, et al., Effects of the phase interface on spallation damage nucleation and evolution in multiphase alloy, J. Alloy. Comp. 740 (2018) 321.
[226] W. Han, M. Kunieda, Wire electrochemical grinding of tungsten micro-rods using neutral electrolyte, Precis. Eng. J. Int. Soc. Precis. Eng. Nanotechnol. 52 (2018) 458.
[227] J. Singh, R.K. Sharma, Multi-objective optimization of green powder-mixed electrical discharge machining of tungsten carbide alloy, Proc. Inst. Mech. Eng. C J. Mech. Eng. Sci. 232 (2018) 2774.
[228] M.A. Singh, S.K. Rajbongshi, D.K. Sarma, et al., Surface and porous recast layer analysis in mu-EDM of MWCNT-Al2O3 composites, Mater. Manuf. Process. 34 (5) (2019) 567.
[229] Y. Feng, Y. Guo, Z. Ling, et al., Investigation on machining performance of micro-holes EDM in ZrB2-SiC ceramics using a magnetic suspension spindle system, Int. J. Adv. Manuf. Technol. 101 (5–8) (2019) 2083.